**This review was conducted by a team of researchers at Queensland University of Technology with broad expertise in materials mechanics, chemistry, and biology.**

Multifunctional nacre-like materials

Seashells and bone have inspired simultaneously strong and tough materials. Translation of these materials to industries requires implementing other functionalities such as transparency, bioactivity, and electromagnetic shielding. This review assesses the progress and outlook in the fabrication, mechanics, and multi-functionality of these bio-inspired materials.
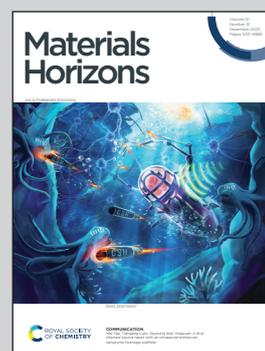
ROYAL SOCIETY OF **CHEMISTRY**

rsc.li/materials-horizons

Check for updates

Multifunctional nacre-like materials

Zizhen Ding, [ab] Travis Klein, [ab] Christopher Barner-Kowollik ID [cde] and
Mohammad Mirkhalaf ID *[abd]

Nacre, the iridescent inner layer of seashells, displays an exceptional combination of strength and toughness due to its 'brick-wall' architecture. Significant research has been devoted to replicating nacre's architecture and its associated deformation and failure mechanisms. Using the resulting materials in applications necessitates adding functionalities such as self-healing, force sensing, bioactivity, heat conductivity and resistance, transparency, and electromagnetic interference shielding. Herein, progress in the fabrication, mechanics, and multi-functionality of nacre-like materials, particularly over the past three years is systematically and critically reviewed. The fabrication techniques reviewed include 3D printing, freeze-casting, mixing/coating-assembling, and laser engraving. The mechanical properties of the resulting materials are discussed in comparison with their constituents and previously developed nacre mimics. Subsequently, the progress in incorporating multifunctionalities and the resulting physical, chemical, and biological properties are evaluated. We finally provide suggestions based on 3D/4D printing, advanced modelling techniques, and machine elements to make reprogrammable nacre-like components with complex shapes and small building blocks, tackling some of the main challenges in the science and translation of these materials.

Wider impact

Diverse applications, including biomedical, transport and electronics, require materials with combinations of low density, high mechanical performance, and other functionalities such as self-healing and transparency. Nacre-like materials in which stiff and strong building blocks are arranged in a brick-wall architecture and joined with deformable interfaces have shown the ability to combine these properties, leading to scientific discoveries with follow-on technological, social, and economic benefits. An example application is bone grafts, the market for which was valued at US\$2.78 billion in 2020 and is expected to reach ~US\$4 billion in 2028. Metal implants currently used to repair damaged/diseased load-bearing bones lack the tissue-regenerating capabilities of bioceramics, yet are preferred because they are tougher. Combining metals and bioceramics in a nacre-like material promises bone grafts with combinations of toughness and tissue integration ability, potentially improving outcomes for millions globally suffering from bone conditions. Similar examples and future directions are discussed for diverse applications in this review article.

1. Introduction

Combining stiffness, strength, and toughness continues to be a critical challenge in materials science and engineering.[1] Natural materials such as silk, bone, and nacre from sea shells have evolved a powerful strategy to solve this challenge:

arranging stiff and strong building blocks into a precision architecture and joining them with deformable biopolymeric interfaces.[2] The building blocks provide stiffness and strength, the interfaces impede crack propagation, and the architecture activates the relative and progressive sliding of the blocks. Together, they result in mechanisms such as crack deflection, crack branching out into multiple paths, and the spread of deformation to large volumes of material, thereby conferring toughness (Fig. 1).[3–5] One of the examples of these natural materials is nacre, the iridescent inner layer of seashells (Fig. 1). Nacre is almost three orders of magnitude tougher than its primary ingredient, aragonite.[6] Its remarkable mechanical performance is attributed to its 'brick-wall' architecture (Fig. 1), where the well-aligned aragonite micro-platelets (95 vol%) work as 'bricks' or 'platelets', and a few per cent of macromolecules as the 'mortar'.[7,8] These macromolecules include a wide range of proteins and polysaccharides.[4,9]

[a] *School of Mechanical, Medical and Process Engineering, Queensland University of Technology (QUT), 4000 Brisbane, QLD, Australia. E-mail: mohammad.mirkhalaf@qut.edu.au*

[b] *Centre for Biomedical Technologies, Queensland University of Technology (QUT), 4059 Brisbane, QLD, Australia*

[c] *School of Chemistry and Physics, Queensland University of Technology (QUT), 4000 Brisbane, QLD, Australia*

[d] *Centre for Materials Science, Queensland University of Technology (QUT), 4000 Brisbane, QLD, Australia*

[e] *Institute of Nanotechnology (INT), Karlsruhe Institute of Technology (KIT), Hermann-von-Helmholtz-Platz 1, 76344 Eggenstein-Leopoldshafen, Germany*

Inspired by the noted brick-wall architecture, also commonly known as nacre-like architecture, fabrication techniques such as 3D printing, freeze-casting, mixing/coating-assembling, and laser engraving have been used to replicate this architecture to generate materials with similar mechanical performance. However, the level of control over the geometry and assembly of the building blocks is usually achieved at the cost of increasing the length scale and working with building blocks typically a few millimetres in size.[11–13] The level of structural organization at the nano/micro-scale and the resulting toughening mechanisms observed in nacre at these small scales have not yet been realized in its synthetic counterparts. Working with large (mm- to cm-sized) building blocks comes at the expense of losing the flaw insensitivity of small (nm- to μm-

sized) blocks, which allows their strength to reach the theoretical strength of a solid.[14,15] In addition to the lack of precise control over the shape and arrangement of blocks at the small scale, it is difficult to scale up nacre-like materials with small building blocks. Moreover, there is still room to improve the architectural complexity and control at the small scale to improve their mechanics.[16,17] Significant research is currently ongoing to address these challenges, and prominent review articles have discussed the progress in the fabrication and mechanics of nacre-like materials.[4,7,18–23] However, the technical advancement over the past few years has not yet been critically evaluated.

While nacre-like materials have proven efficient in combining strength and toughness, their efficiency in yielding other

Zizhen Ding

Zizhen Ding graduated with a bachelor's degree (First class honours) in Biomedical Engineering from the University of Sydney and is now a PhD student under the supervision of Dr Mohammad Mirkhalaf in the School of Mechanical, Medical and Process Engineering at the Queensland University of Technology. His research interest is in the area of 3D and 4D printing of ceramics, focusing on works to make tougher (less brittle) ceramics and form ceramics into complex shapes without sacrificing their mechanical properties.

Travis Klein

Travis Klein is a Professor in the Mechanical, Medical, and Process Engineering School at the Queensland University of Technology (QUT). He earned a PhD in Bioengineering from the University of California San Diego in 2005. Travis leads the Cartilage Regeneration Laboratory, and focuses primarily on developing biomaterials, biofabrication approaches and mechanical stimulation technologies for tissue engineering and regenerative medicine. In 2020, he founded QUT's Centre for Biomedical Technologies, a multidisciplinary centre aiming to deliver better health in our lifetime, by improving how we treat complex medical cases stemming from injuries, infection and age-related issues.

Christopher Barner-Kowollik

A PhD graduate of Göttingen University, Germany, Christopher Barner-Kowollik joined the University of New South Wales in early 2000 rising to lead the Centre for Advanced Macromolecular Design as one of its directors. In 2008, he joined KIT, establishing a German Research Council (DFG) funded Centre of Excellence. He moved to QUT in 2017, establishing QUT's Soft Matter Materials Laboratory. Over his 24 year career to date focussing on (macromolecular) photochemical processes, he supported highly collaborative large teams. His multi-award-winning research explores precision orthogonal, synergistic and antagonistic photochemical reactions and their application in macromolecular systems.

Mohammad Mirkhalaf

Mohammad Mirkhalaf studied at McGill University (PhD), Nanyang Technological University (Master's), and Isfahan University of Technology (Bachelor's). After obtaining PhD in 2015, he has worked at the National Research Council of Canada, the University of Sydney, and the Queensland University of Technology. Over the past decade, he and colleagues have established several initiati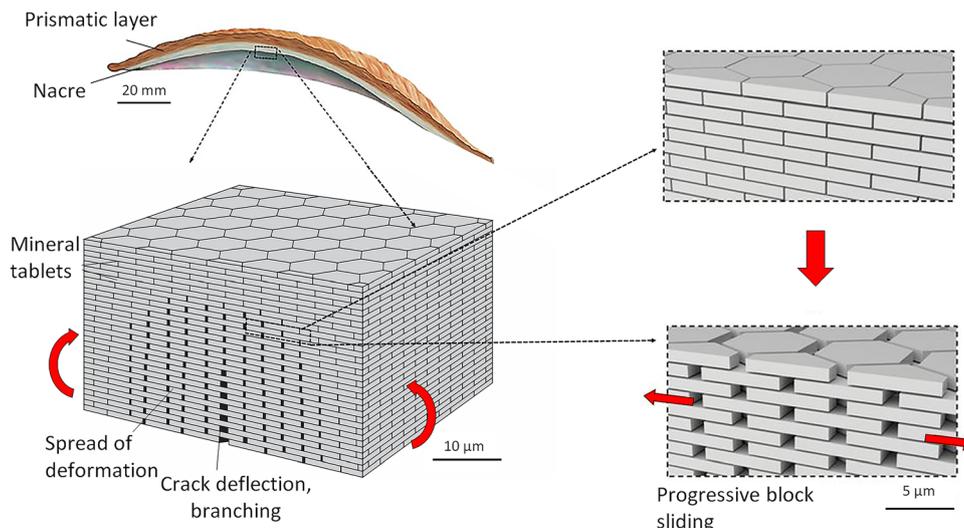ves to develop advanced mechanical metamaterials and understand their physical, chemical, and biological behavior, including their interactions with tissues.

Fig. 1 Schematic of Nacre's brick-wall architecture and the prevailing toughening mechanisms. Reproduced from ref. 4 and 10 with permission from Springer Nature, copyright 2020, and the American Association for the Advancement of Science, copyright 2019.

functionalities has been questioned and explored in recent literature. Translation of these materials to real-life applications often requires a combination of excellent mechanical properties and other functionalities such as self-healing,[24] force sensing,[25] bioactivity,[26] transparency,[10] heat conductivity and resistance,[27] and electromagnetic interference shielding.[28] For example, whether heat resistance and electromagnetic shielding can be incorporated jointly in nacre-like materials to be used as flexible electronics is currently under discussion.[29] Critically, an assessment of the development and fabrication of nacre-like materials with multifunctionalities is missing. The current review fills these gaps. We confined our review to the following definition of nacre-like materials: composites of stiff and strong platelets arranged in a staggered architecture that interact through energy-dissipative interfaces. The platelets can be 2D or 3D. The thickness of 2D platelets, such as graphene, is commonly almost three orders of magnitude smaller than their lateral dimensions; 3D platelets have a characteristic thickness 10–40 times smaller than their lateral dimensions.

We begin our review by presenting the recent advances and achievements in the fabrication and mechanics of nacre-like materials developed through 3D printing, freeze-casting, mixing/coating-assembling, and laser engraving in the 2020s. Subsequently, we explore in detail the requirements and approaches to use nacre-like materials in real-life applications with different multifunctionalities in dedicated sections summarized in Fig. 2. Finally, we provide suggestions based on nanoscale printing and modelling techniques to address the challenges of nacre-like materials in the future.

2. The advancement of mechanics and fabrication techniques

A wide array of fabrication techniques has been employed to generate nacre-like materials. In the subsequent section, we highlight the advancement of the most commonly used techniques in the past three years.

2.1. 3D printing (additive manufacturing) (Fig. 3(a))

In nacre-like materials, like other architectured materials (also known as mechanical metamaterials), the internal architecture governs the function.[22,32] As such, free-form fabrication techniques that can offer close control over the internal architecture come of great interest. Various 3D printing approaches have been explored to make nacre-like materials in the last three years. These approaches can be categorized into two main groups: (i) photopolymerization (such as stereolithography and digital light processing) and (ii) material Extrusion with hard (ceramics) and soft (polymers) dispensed through a nozzle. In these fabrication techniques, a 3D virtual object is first sliced into layers using computer software. A 3D printer subsequently constructs these layers in a sequential manner, either by depositing a thermoplastic resin through a nozzle on a platform or immersing a build platform in a vat of polymers and moving the object being made upwards after each new layer is cured.[33,34] Ultraviolet (UV) light is the most common lighting source used to cure layers of photosensitive polymers sequentially.

To achieve the desired 'brick-wall' architecture using 3D printing, two general pathways have been followed. The first has been to align nano/micro-sized platelets ('bricks') within a resin using different 3D printing techniques. The more recently developed second way has been to print the building blocks and architecture simultaneously to achieve a higher level of control over the shape and arrangement of blocks, albeit currently at the expense of losing the benefits of nano/micro-scale size of blocks. In the first set of approaches, different types of forces have been employed to align platelets ('bricks') across various 3D printing techniques with a photopolymer resin acting as the fixative mortar. The polymeric mortar is then
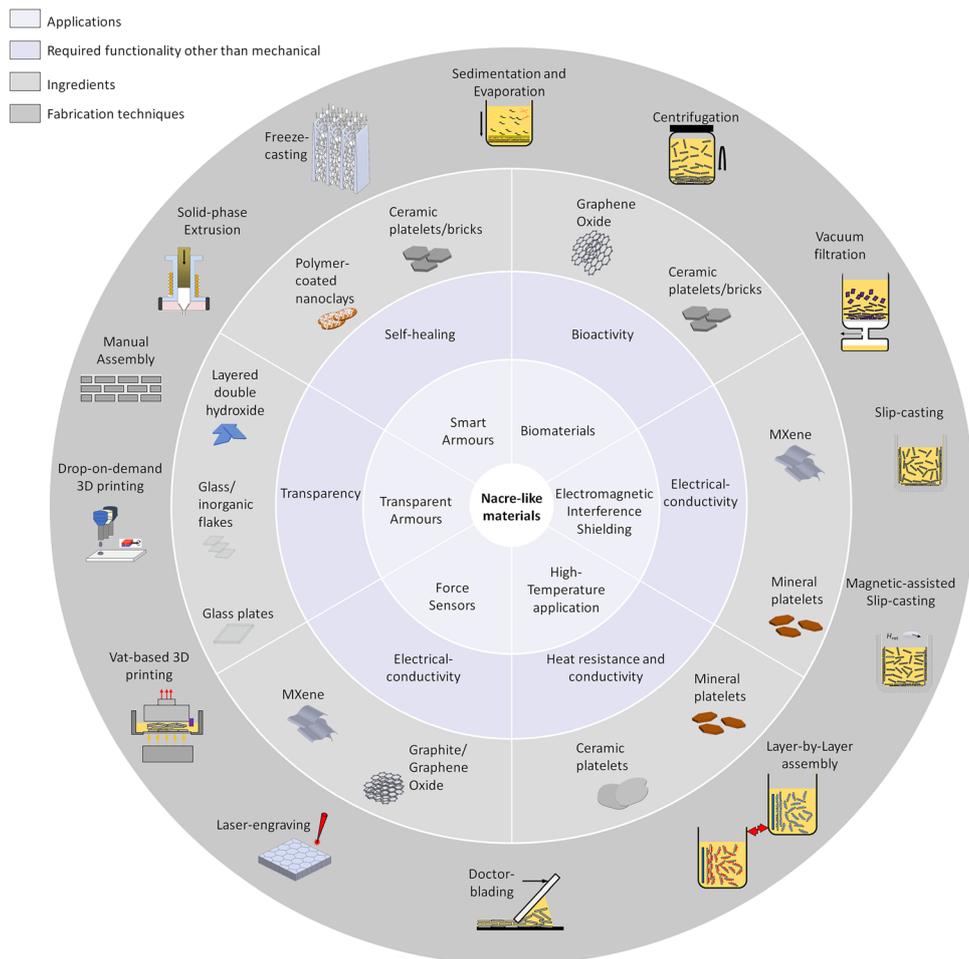
Fig. 2 Graphical summary of the main applications for which nacre-like materials have been used to date. The functionality required for the particular application, the ingredients used, and the main fabrication techniques are summarized. MXene is a class of 2D transition metal carbides and/or nitrides. Some of the schematics of the fabrications techniques are reproduced from ref. 4 with permission from Springer Nature, copyright 2020.

solidified to fix the platelets in place using UV curing in photopolymerization-based printing and thermosetting and thermoplastic effects in extrusion-based techniques. Additives such as calcium oxide (CaO) and silica (SiO_2) particles have been doped into the polymeric mortar containing ceramic platelets, and the subsequent sintering process results in the growth of the platelets. This process is also known as the grain growth process, which helps the platelets to grow into a nacre-like architecture.[35]

The compressive forces generated during layer formation in photopolymerization-based printing,[36] and the shear forces generated within the nozzle in extrusion-based printing,[37] contribute to the alignment of these platelets. External magnetic and electric forces have been used to further align the platelets in the photopolymer resin during the printing process.[38,39] However, the level of control over the platelets' alignment is restricted to printing resin with low platelets solid content and mechanical properties remained inferior compared to the nacre at high concentrations. To address this challenge, a custom-built stereolithographic 3D printer was developed in which each layer (composed of resin and platelets)

is deposited using doctor blading. Doctor blading has been previously used to generate nacre-like films[40,41] but not combined with 3D printing to make bulk components. In analogy to how a knife spreads butter onto bread, the shear forces generated between the blade and the bottom of a vat that contains the resin-platelets mixture have allowed a nacre-like material containing 55 wt% boron nitride (BN) nano-platelets to successfully align prior to the UV curing process (Fig. 4(a)).[42] The custom-built printer offered the ability to customize the rotation speed of the vat and the thickness of the printing layers. By using optimum vat rotation speeds, the shear forces were maximized between the blade and the bottom of the vat without breaking the film, which resulted in the successful alignment of BN nano-platelets with high solid loading. The 3D printed nacre-like material was around 6 times stronger (143 MPa) and around 3 times tougher (2.53 MPa m$^{1/2}$) than the same architecture made with only printing resin (Fig. 4(a)).[42]

An alternative recently developed approach to control the alignment at high platelet concentrations is by combining a drop-on-demand 3D printing and a magnetic-assisted alignment technique. During the fabrication process, ink droplets
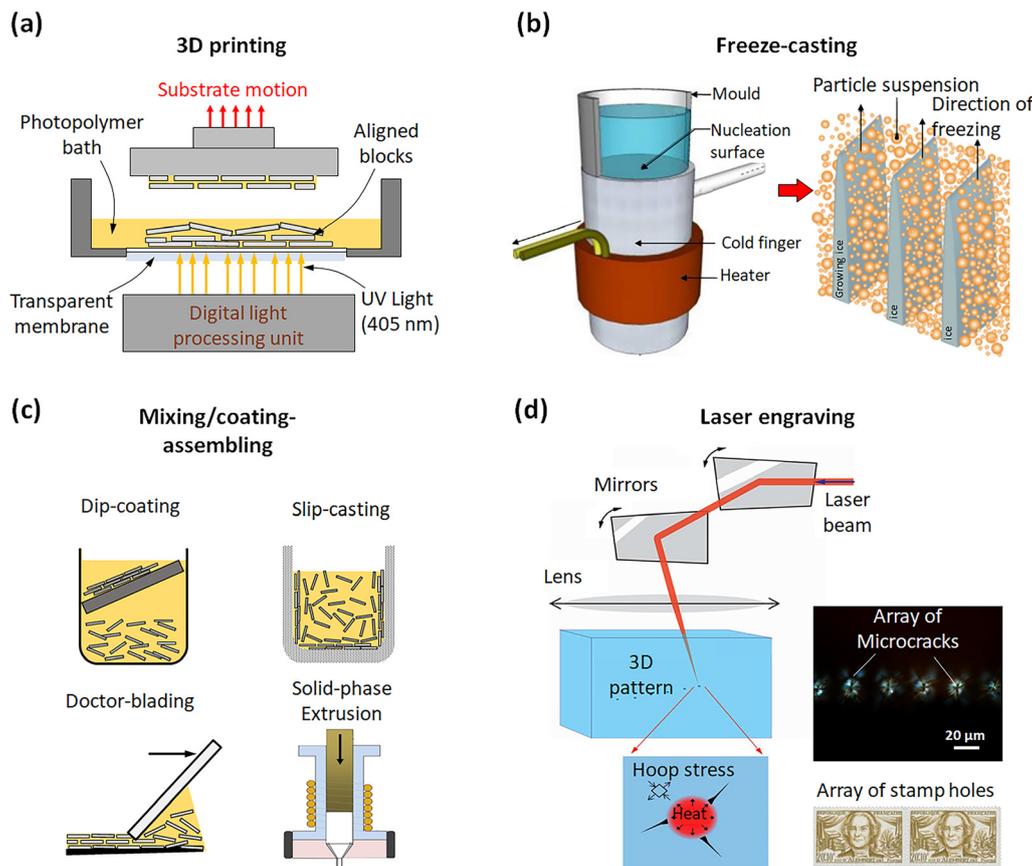
Fig. 3 Commonly applied fabrication techniques to achieve nacre-like materials. (a) 3D printing, (b) Freeze-casting, (c) Mixing/coating-assembling, and (d) Laser engraving. Images (a), (c), and (d) are reproduced from ref. 4, and 30 with permissions respectively from Springer Nature, copyright 2020, and Springer Nature, copyright 2009. Image (b) is reproduced from ref. 7 and 31 with permissions respectively from Springer Nature, copyright 2014 and the American Ceramic Society, copyright 2009.

consisting of magnetically active xirallic titania-coated alumina microplatelets and polyvinylpyrrolidone (PVP) aqueous solution were initially deposited onto the substrate and immediately manipulated by the magnetic field to form an aligned lamellar architecture. The ink droplets then subsequently underwent natural sedimentation and evaporation, followed by sintering and infiltration of polydimethylsiloxane (PDMS), enabling the development of a nacre-like material with a volumetric solid concentration of up to 50 vol% (Fig. 4(b)).[43] By varying the strength of the magnetic field, the orientations of the platelets could be adjusted, and consequently, the material's mechanical properties could be tuned. The material with an alignment angle of $0°$ was 1.3 times stronger (~ 5 MPa) and could dissipate 26 times more energy (361 kJ m^{-3}) than material with $90°$ alignment (Fig. 4(b)). The material with platelet angles between $0°$ and $90°$ had mechanical properties between these two extremes.[43] This is similar to the Voigt and Reuss composites, which establish the upper and lower bounds for the modulus of composites.[45]

The common challenge in these techniques is the low level of control over the shape and arrangement of building blocks. The emergence of ceramic photopolymerization techniques provided opportunities to address this challenge by printing both the shape and arrangement of the building blocks simultaneously.[44] Thus, the shape of the building blocks is not restricted to platelets, and full control over how the blocks are arranged can be achieved. Building block shapes such as square, rectangular, circular, and hexagonal have been recently explored using a commercially available 3D printer and ceramic resin, followed by the ceramic sintering process (Fig. 4(c)).[44] The architecture was then put onto a spring-driven centrifugal casting machine, where the spring was tensioned. The aluminium alloy was then melted using a handheld torch and poured into the scaffolds. Finally, as the tension was released in the casting setup, the centrifugal forces drove the molten aluminium alloy to infiltrate through the previously made architecture to form the nacre-like ceramic/metal material. The strength of material with prismatic-shaped architecture was 7.4 times stronger (130 MPa) than the same architecture made of pure ceramic and obtained toughness up to 8.49 MPa m$^{1/2}$ (Fig. 4(c)).[44]

2.2. Freeze-casting (Fig. 3(b))

During the formation of sea ice, ice crystals expel salt and other molecular components from the water and trap them between the crevices of growing crystals.[46] Inspired by this
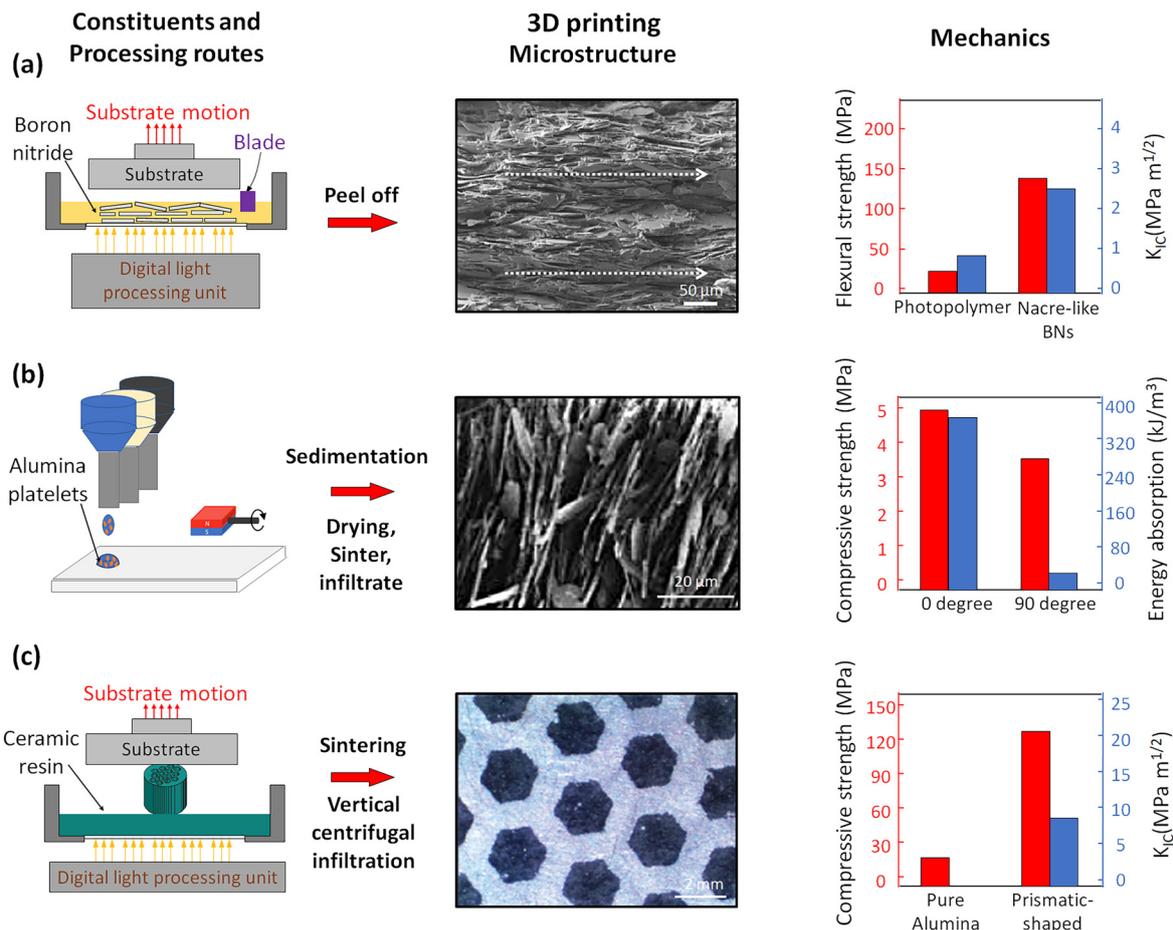
Fig. 4   The constituents, processing routes, microstructure, and mechanical properties achieved by (a) a custom-made 3D printer, (b) the combination of drop-on-demand 3D printing and magnetic-assisted assembly, and (c) a commercial 3D printer. Images (a) and (b) are adapted from ref. 42 and 43. Image (c) is reproduced from ref. 44 with permission from Wiley-VCH GmbH, copyright 2021.

phenomenon, the freeze-casting (or ice-templating) method was adopted for nacre-like materials.[47–50] Four steps are commonly involved: (i) a ceramic slurry is poured into a mould placed at the top of a copper rod (finger), through which liquid nitrogen runs. The solidification front of the freezing ice crystals formed by the finger expels the solid contents within the slurry and forms a lamellar architecture; (ii) the forming ice is sublimated by freeze-drying in a vacuum; (iii) the lamellar architecture is solidified by sintering; (iv) the sintered sample is infiltrated with a polymer or metal to generate a layered architecture. Compressing this layered architecture can result in the 'brick-wall' architecture.[51–53] During unidirectional freeze-casting, ice crystals nucleate on a flat plate and form along a single freezing direction without any controlled orientations in other directions. Hence, only a multidomain short-range lamellar architecture can be observed. To address this challenge, a sloped wedge, rather than a flat plate, is placed on the bottom surface so that the ice crystals nucleate and grow in a direction both perpendicular and parallel to the flat bottom of the mould. Consequently, the slurry can be frozen into a long-range monodomain lamellar architecture.[54] This adapted technique is called bidirectional freezing, as opposed to the more conventional unidirectional freezing.

Although bidirectional freeze-casting can produce long-range monodomain lamellar architecture, it still features the size limitation of either its corresponding mould or PDMS wedge length to scale up the fabrication process.[55] Thus, a recent freeze-casting process was designed to achieve a nacre-like material with a long-range monodomain lamellar architecture without size limitations (Fig. 5(a)).[56] The architecture was achieved by manipulating the wettability of the copper mould's surface before pouring the ceramic slurry and placing it onto the copper rod (finger). Classical ice nucleation theory indicates that surface wettability is proportionally related to the ice nucleation rate. Thus, by programming the mould surface with a linear wettability gradient, rows of ice crystals grow successively from where the surface is highly hydrophilic to where the surface is hydrophobic and trap particles in the direction perpendicular to the gradient, ultimately forming the long-range monodomain lamellar architecture after sublimation (Fig. 5(a)). Furthermore, as this technique is an extrinsic modification of the traditional freeze-casting method, the
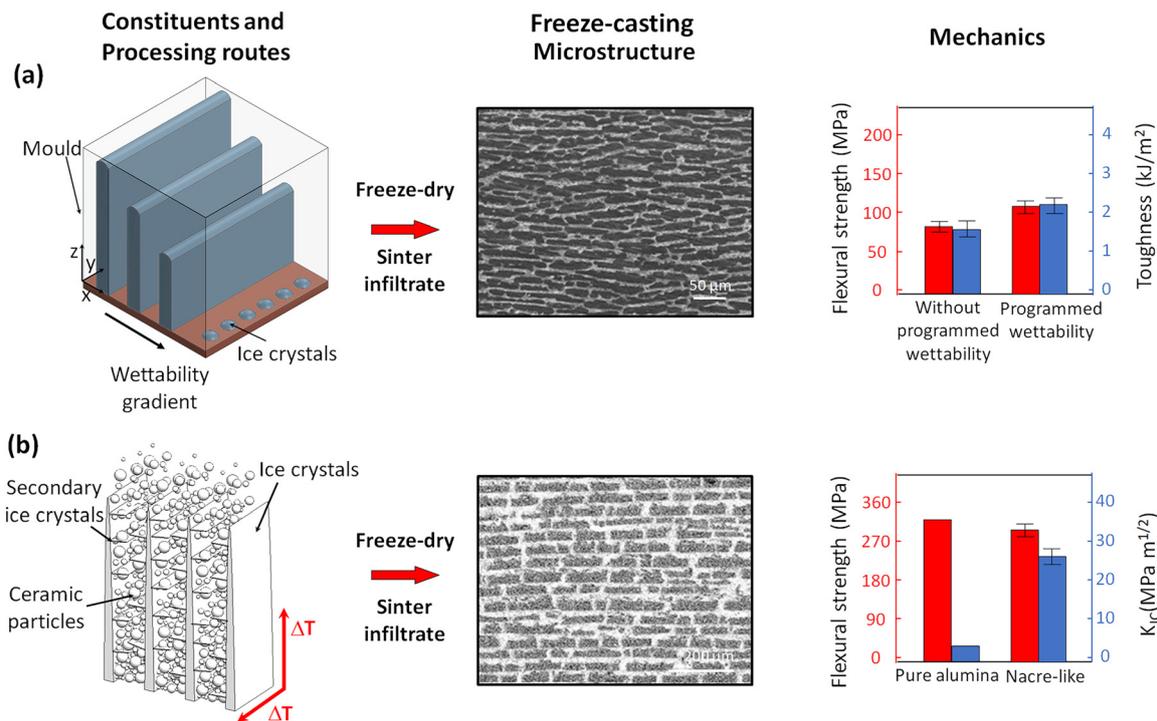
Fig. 5 The constituents, the processing routes, the microstructure, and the mechanical properties achieved by (a) the freeze–casting process with designed linear wettability and (b) the freeze–casting process that takes advantage of the secondary ice crystal formations. Image (a) is adapted from ref. 56, and image (b) is reproduced from ref. 57 with permission from Elsevier Ltd, copyright 2022.

fabrication can scale up without the size limitations by simply dipping a well-insulated mould at any size with surface modifications into a cold bath (usually at −60 °C). Finally, the formed architecture could be further toughened by infiltrating the layered architecture with polymethyl methacrylate (PMMA) after the sublimation and sintering process. The produced material was around 1.5 times stronger (108.9 ± 7.5 MPa) and around 1.2 times tougher (2232 ± 295 J m^{-2}) than the forming material without programmed wettability (Fig. 5(a)).[56]

Regardless of the different freeze-casting procedures, one of the issues with freeze-casting for manufacturing nacre-like materials is that during the freeze-casting, secondary ice crystals form and grow perpendicular to the freezing direction due to the instability of the solid–liquid interface of the freezing front.[55,58,59] These cracks could severely decrease the mechanical strength of the architecture and thus are commonly perceived as undesired. However, recent research has found that these cracks can be useful for segregating the ceramic particles into 'bricks' with both unidirectional freeze-casting and bidirectional freeze-casting procedures (Fig. 5(b)), where the height and aspect ratio of these 'bricks' are proportionally related to the size of the ceramic particles.[57,60] After the sublimation and sintering process, these cracks can also serve as 'mortar' phase infiltration channels, which in this case, aluminium was chosen as the infiltration material to make the ceramic/metal composite with nacre-like architecture. The produced material with the bidirectional freeze-casting procedure was up to 8 times tougher (28.5 ± 1.0 MPa m$^{1/2}$), and its flexural strength

was almost equivalent to that of pure alumina (294 ± 8 MPa) (Fig. 5(b)).[57] Nevertheless, how to control the size of these 'bricks' precisely is not clear. Thus, further investigations are necessary to clarify this aspect.[60]

2.3. Mixing/coating-assembling (Fig. 3(c))

Ceramic or mineral platelets with high aspect ratios[61,62] can be mixed and coated with metals,[63] polymers,[64–70] or ceramics[62] using electrostatic coating,[62] sol–gel methodologies,[71] and spin-coating[72] to form the building blocks that can be then assembled into nacre-like materials. The assembly techniques include sedimentation/evaporation,[73] slip-casting,[61] centrifugation,[11] vacuum filtration,[29,74–78] doctor-blading,[79] solid-phase extrusion,[27] dip-coating,[80] or manual assembly.[24] Like other fabrication techniques, many researchers used these assembly techniques to make nacre-like materials, as detailed in previous review articles.[4] Here, we restrict ourselves to exploring selected assembly techniques (Fig. 3(c)). Dip-coating involves immersing a substrate in the platelets mixture, akin to dipping a chicken wing into a bowl of dipping sauce and slowly pulling it out, assembling a thin layer of platelets onto the substrate. Doctor-blading uses a blade to spread the mixture onto a substrate, aligning the platelets. Slip-casting involves layering the platelets onto the wall of a porous mould through the continuous removal of the liquid phase through tiny pores. Finally, solid-phase extrusion involves consolidating a mixture of ingredients under high temperature and pressure to generate a solid column, followed by extrusion through a nozzle. In

the initial studies using these techniques for nacre-like materials, the assembly process was mostly driven by gravitational force, surface energy minimisation, centrifugation, atmospheric pressure and natural evaporation.[81] Magnetic and electrical forces were subsequently employed in addition to these procedures to control the orientation of the platelets.[63,82–84] Post assembly, the metal- and ceramic-coated platelets are joined using either hot compression[85] or spark plasma sintering.[63,86,87] Assemblies made of polymer-coated platelets do not necessarily need to be further processed, as the hydrogen and electrostatic bonds keep the assembly stable. Mixing/coating-assembling approaches offer better control over the shape of building blocks than freeze-casting methods. However, arranging the building blocks in a controlled architecture, such as the brick-wall architecture with a precise offset between layers is difficult. Thus, the recent advances were primarily focused on how mixing/coating-assembling approaches could be used to achieve nacre-like materials with different multifunctionalities, rather than nacre-like materials with precise architecture. The multifunctionalities will be discussed in the next section.

2.4. Laser engraving (Fig. 3(d))

Laser engraving consists of guiding and focusing nanosecond laser pulses through mirrors and a focal lens to a specific focal point within a transparent material such as glass or on the surface of opaque materials such as ceramics.[88] At the focal point, the heat is locally generated, resulting in local expansion, hoop stresses, and, consequently, microcracks. Arrays of thousands of microcracks can be generated within minutes to form weak interfaces with well-designed shapes, analogous to natural materials' weak interfaces. Like arrays of stamp holes, weak 3D interfaces can be engraved within transparent materials like glass. These interfaces are designed to be sufficiently strong to hold the piece together but also sufficiently weak to break upon loading, dividing the material into building blocks. The laser light cannot access the inner parts of opaque materials. So, instead of engraving an array of 3D defects within the material, cuts that do not go through the entire thickness of the materials can be embedded in opaque materials. Similar to the array of microcracks, these partial cuts can also break upon loading, leading to architectured ceramics.[88,89]

The designed weak patterns can be a nacre-like pattern, yielding a nacre-like material. The separate blocks subsequently interact with each other through friction.[30,90] Alternatively, the interfaces can be infiltrated with a tougher phase, in which case the blocks interact through this second phase.[30,91] Or patterns of weak interfaces can be engraved within each layer, and the layer can then be laminated with a tougher phase in between to make the nacre-like material.[10] In one example, a focused pulsed laser beam was used to 3D engrave hexagon-shaped weak interface onto the glass sheets, followed by stacking the designed layers with an equal offset to resemble the 'brick-wall' architecture of the nacre (Fig. 6(a)). Soft ethylene-vinyl acetate (EVA) or Surlyn (an ionomer) layers were intercalated uniformly between hard layers. The entire architecture was finally compressed at a constant temperature. During the compression process, the hard glass layers broke along the weak interfaces to form the 'bricks', and the soft polymer layer was partially melted and infiltrated through the separated
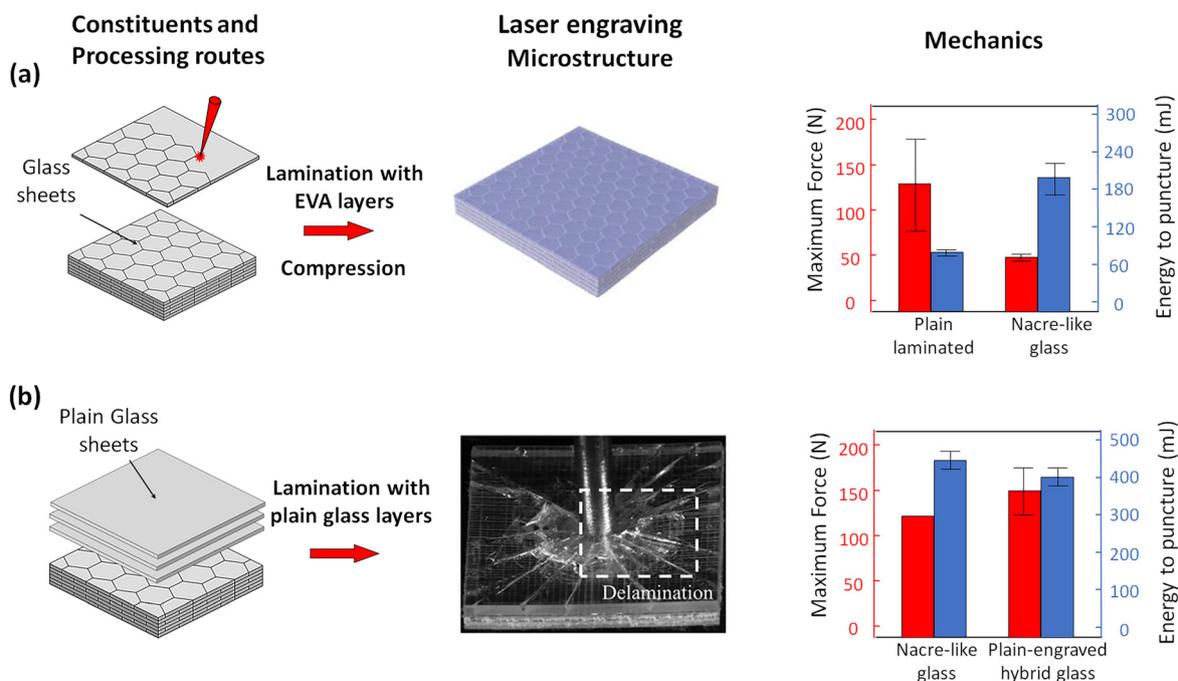
Fig. 6 The constituents, the processing routes, the microstructure, and the mechanical properties achieved by (a) the laser–engraving process. and (b) the combination of laser–engraved and plain glass sheets. The images are reproduced from ref. 4, 10 and 92 with permissions respectively from Springer Nature, copyright 2014, the American Association for the Advancement of Science, copyright 2019, and IOP Publishing Ltd, copyright 2021.

interfaces to form the 'mortar'. Such an architecture absorbed almost 3 times more impact energy ($\sim$220 mJ) than pure laminated glass with the same constituents and compositions. However, this improved toughness came at the expense of losing strength and stiffness, where the strength of the architecture was 2.6 times weaker than pure laminated glass ($\sim$50 N in maximum puncture force) (Fig. 6(a)). To improve the stiffness and strength of these nacre-like glasses, one or more layers of plain glass were added on top of engraved laminated glass, like the hard prismatic calcite layers of seashells. As a result, the nacre-like glasses with one plain glass layer was almost 3 times stronger than that with only engraving layers.[10]

More recently, different arrangements between the plain glass layers and the engraving layers and the effect of individual plain glass layer thicknesses on enhancing stiffness have been discussed in more depth (Fig. 6(b)).[92] When the overall thickness of the glass panel is constant, increasing both the number and thickness of the plain layers improved the maximum puncture force by up to 1.3 times (150 N) and stiffness by up to 5.2 times ($\sim$800 N mm^{-1}). However, because of a lower number of engraved layers present in the design to absorb energy through platelets sliding, the energy absorption level of the glass panel with a plain-engraved hybrid design was up to 1.2 times inferior to the glass panel with only engraved layers (Fig. 6(b)).[92] In addition, replacing multiple individual plain layers with a single thick plain glass decreased the energy absorption capacity. This phenomenon can be explained by the less sliding occurring between the layers upon impact, which results in smaller energy absorption (Fig. 6(b)).[92]

We provided a flexural strength – initiation toughness map of nacre-like materials in our previous review on the subject.[4] A more comprehensive version, including the studies over the past three years, is provided here (Fig. 7). Table 1 summarizes the materials and fabrication techniques recently used for nacre-like materials and the resulting mechanical properties.

The conventional trade-off between strength and toughness observed in synthetic materials is absent in nacre-like materials. However, most fabricated nacre-like materials are still limited to the initiation toughness of 13 MPa m$^{1/2}$. To push the mechanical performance achieved with current nacre-like materials, there are four major factors to consider: (i) the size of the building blocks; (ii) the level of control over the geometry of the building blocks; (iii) the precision of the architecture; and (iv) the level of control over the material properties of the different phases and at different length scales within the architecture. Small building blocks are useful because they tend to have smaller defects and, consequently, higher strength.[15] Freeze-casting can assemble small building blocks on the nano/micrometre scale, but the geometry of these building blocks cannot be precisely controlled. While the thickness of layers (and consequently the platelets) is to some extent controlled in the freeze-casting process, the lateral dimensions of the platelets are either controlled by the physics of ice-formation or fracture of the layer under compression post-casting. As a result, precisely defined overlaps between the building blocks have not been achieved. Mixing/coating-assembling can offer better control over the geometry of the building blocks at the same size scale. However, achieving full control over the arrangement of the building blocks at small scales in bulk functional materials using controlled assembly or self-assembly methods has been challenging.[93] Laser engraving can provide excellent control over the geometry of the blocks and their arrangement. However, the size of microcracks formed by the current nanosecond laser pulse is between 10–50 μm in glasses and ceramics, preventing the creation of building blocks smaller than 100 μm.[30] In addition, the laser engraving technique can only be used for non-interpenetrating building blocks.

3D printing a mixture of platelets in a resin allows the size and geometry of the platelets to be predetermined, yet the

Fig. 7 The more completed toughness–strength Ashby chart for nacre-like materials in flexion. The data points in the figure are from ref. 13, 42, 47, 48, 51, 53, 57, 55, 60, 61, 63, 82, 85, 86, 94–97.

Table 1 Summary of the fabrication methods, constituents, and mechanical properties of obtained nacre-like architectures. σ_s is the strength of the materials; K_{IC} is the critical stress intensity factor for crack initiation

Fabrication method	Constituents	Architecture	Test condition	σ_s (MPa)	K_{IC} (MPa m$^{0.5}$)
Freeze-casting	Alumina – Silica Calcia[55]	Nacre-like	Flexion/Tension	470	6
	Alumina – Al Ti[47]			600	6
	Alumina (or SiC) – Al Mg[97]			730	12.5
	Alumina – Al Si[53]			360	6
	Alumina – PMMA[48]			200	3
	Alumina – metallic glass[13]			800	5.5
	Alumina-Aluminium[57]			294	7.2
	Titanium dioxide –Aluminium alloy[60]			357	7.39
Mixing/coating-assembling	Glass – methacrylate[94]	Nacre-like	Flexion/Tension	80	0.7
	Alumina – nickel[86]			200	2
	Alumina – SiO$_2$[61]	Nacre-like (complex shapes)	Flexion	600	6
	Alumina – nickel[63]			320	10
	Alumina – Al borate[82]			650	7.2
	Alumina – nickel[85,98]	Nacre-like	Flexion	480	3.5
Laser engraving	Glass – polyurethane[91]	Nacre-like	Puncture	4–40	1.2
	Borosilicate glass (or alumina) – Surlyn[10,99]		Impact		
3D printing	Boron nitride[42]	Nacre-like	Flexion	143	2.53
	Ceramic – Aluminium alloy[44]			295.4	8.49

overlap between the platelets in the neighbouring layers remains largely uncontrollable. 3D printing of the building blocks and architecture simultaneously affords full control over the geometry and architecture, but it is achieved at the expense of tying the size of the blocks to the resolution of the 3D printing processes. The printing processes so far used for these purposes yielded block sizes in the range of 2–4 mm, close to 100 times larger than the block sizes achieved with other manufacturing techniques such as freeze-casting. The lack of control over the geometry and assembly of the building blocks in nacre-like materials at small scales also limits the type of interfacial interactions between building blocks, which further limits the range of toughening mechanisms that can be implemented to enhance the current mechanical properties. For example, spread-of-deformation and process-zone-toughening mechanism have been obtained in nacre-like materials made of mm-sized building blocks,[10] but these mechanisms are largely absent when smaller building blocks are used. There thus still exists a need for a fast and scalable fabrication approach that can yield mechanically functional bulk nacre-like materials made of nano/micro-sized blocks with full control over the architecture and properties of the phases.

3. Incorporating multi-functionalities

In Section 2, we showed that duplicating the structure and mechanics of nacre results in combinations of mechanical stiffness, strength, and toughness not seen in traditional monolithic materials. This outstanding mechanical performance makes nacre-like materials attractive for various applications. However, translation of these materials for most applications necessitates functionalities other than mechanical properties. A significant amount of research has been dedicated to incorporating these multifunctionalities in nacre-like materials over the past decade. In the following section, we will review the most common functionalities incorporated in nacre-like materials, namely self-healing, force sensing, bioactivity,

heat conductivity/resistance, transparency, and electromagnetic interference shielding.

3.1. Self-healing

Self-healing is observed in many natural materials and is desired in synthetic materials, including nacre-like materials. However, the strong and permanent molecular interactions within most 'mortar' ingredients hinder the molecular mobility of the soft polymer chains, limiting the self-healing potential of these materials. Researchers have come up with three categories of solutions to this problem by using: (1) the Diels–Alder moieties into the polymeric network to incorporate reversible covalent bonds; (2) copolymers as the mortar phase, in which molecules interact mostly through hydrogen bonds that can break and reform; and (3) hook-and-loop adhesive between the platelets to incorporate geometrical reversibility.

The chemical bonds' reversibility underpinned by the Diels–Alder reaction resulted in reforming the chemical bonds after breakage and, in turn, self-healing.[100] To construct the nacre-like architecture, alumina platelets ('bricks') were assembled using bidirectional freeze-casting, followed by infiltrating with the Diels–Alder polymer network ('mortar').[49] The self-restoration behaviour of the material was exemplified by regaining its initial shape under a 50 g load when heated to 120 °C after being temporarily shaped at 60 °C (Fig. 8(a)). The thermal reversibility of the Diels–Alder-driven reversible polymer network enabled the self-healing behaviour, as cracks formed at ambient temperature disappeared upon reheating at 120 °C within 3 minutes (Fig. 8(a)). The heating caused the polymer network to chemically debond, flow into the cracks, and reconnect upon thermal curing.[49]

While self-healing behaviour can be incorporated into nacre-like materials by introducing polymers with dynamic covalent interactions (such as those based on reversible Diels–Alder chemistry), triggering the interactions often requires external stimuli such as heat,[102] water,[103] or ultraviolet (UV) light.[104] To provide autonomous self-healing behaviour, polymer motifs
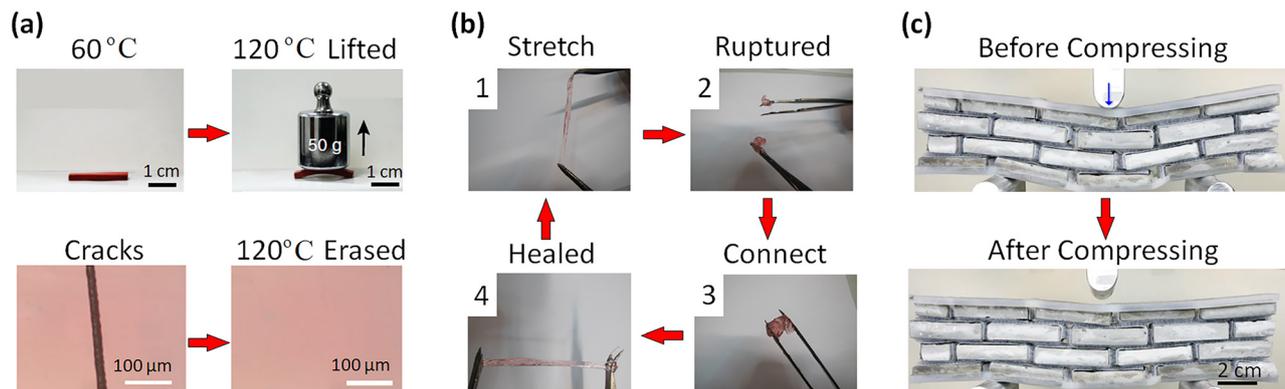
Fig. 8   Self-healing behaviours with (a) a nacre-like architecture based on a dynamic polymer network, (b) the UPy-units doped OEGMA copolymers, and (c) nacre-inspired cement-like materials. Image (a) is adapted from ref. 49. Images (b) and (c) are reproduced from ref. 101 and 24 with permissions respectively from WILEY-VCH Verlag GmbH & Co. KGaA, Weinheim, copyright 2015 and from Elsevier Ltd, copyright 2021.

that form hydrogen bonds within the copolymers were used as the 'mortar' material. For example, 2-ureido-4-pyrimidinoe (UPy) doped poly(oligoethylene glycol methacrylate)-based (OEGMA) copolymers (EG-UPy) ('mortar') and sodium fluorohectorite (NHT) nanoclays ('bricks') were co-assembled into a self-repairing nacre-like film through natural sedimentation and evaporation.[101] UPy was selected as a structural motif as it forms hydrogen bonds within the copolymers and provides the required reversibility for autonomous self-healing.[105–107] NHT nanoclays were chosen as they feature a planar shape with a high-aspect ratio, facilitating material assembly.[108] The autonomous self-healing behaviour of the film was demonstrated by the immediate healing of the EG-UPy copolymer after it was ruptured into two separate pieces in ambient conditions (Fig. 8(b)).[101]

Self-healing can also be incorporated simply by using hook-and-loop adhesives between the blocks.[24] The hook-and-loop adhesive was attached to each side of the cement building blocks using super glue. These blocks were subsequently assembled manually, similar to building with Lego bricks, to form the nacre-like architecture. Rubber layers were then synthesized on both the top and bottom surfaces of the entire architecture using the mould-casting method with a silicone resin (Ecoflex 00-30). The rubber layers were used here to offer the elastic recovery needed for materials to self-heal.[109] The material demonstrated the ability to restore its original shape after cycling loads were applied to both the top and bottom sides regardless of the force directions (Fig. 8(c)). This self-restoration behaviour is due to the hook-and-loop mechanism in the adhesive, which rapidly re-establishes upon contact and the high toughness of the rubber layers. In addition, as the material was constructed by manual assembly, when one or multiple cement bricks were cleaved during mechanical loading, the bricks were replaced, and identical mechanical properties were restored.[24]

3.2. Force sensing

Preventing unpredictable catastrophic failure of structural components is important, particularly for applications in

aerospace and civil infrastructures such as bridges and dams.[110] Current strategies to address this issue still rely on human inspection and manual replacement of the damaged components, which is often time-consuming and inefficient. Consequently, considerable efforts have been devoted to developing force sensing materials that can assess and transmit structural information in real time and self-report the damage of the load-bearing structural components.[111,112] In nacre-like structural materials, introducing 'brick' materials with piezo-resistive properties such as MXene[25] and graphene oxide micro/nano-platelets (GO),[38] have been used to incorporate force sensing. Silk fibroin and polydimethylsiloxane (PDMS) have been used as the 'mortar'.

For example, a nacre-like scaffold with force sensing ability was fabricated by assembling a mixture of MXene nanosheets, silk fibroin, and graphene oxide (GO) platelets using the bidirectional freeze-casting technique.[25] The force sensing capability of the materials was tested by connecting the fabricated scaffold to an LED with a circuit. Since MXene nanosheets are highly electrically conductive, the electrical resistance of the material decreases when the scaffold is compressed as a result of increasing contact areas of the MXene nanosheets. Consequently, the brightness of the LED increases with compression and decreases with decompression (Fig. 9(a)). Moreover, when connecting the scaffold to human facial muscles, the slightest muscle movement was reflected in the output resistance, which further confirmed the pressure-sensitivity of the nacre-like material (Fig. 9(a)). However, the range of pressure that could be applied to the scaffold is limited to pressure range < 5 kPa due to the low solid loading of the solid materials.[25]

To resolve the limited pressure range, a nacre-like material with a volumetric solid concentration of up to 50 vol% was made by the combination of magnetic-assisted assembly and drop-on-demand 3D printing.[43] By using graphite microplatelets as the 'brick' material, the nacre-like material was electrically conductive. Consequently, the force sensing capability of the material was demonstrated by attaching copper plates to the material and measuring the electrical resistance before and
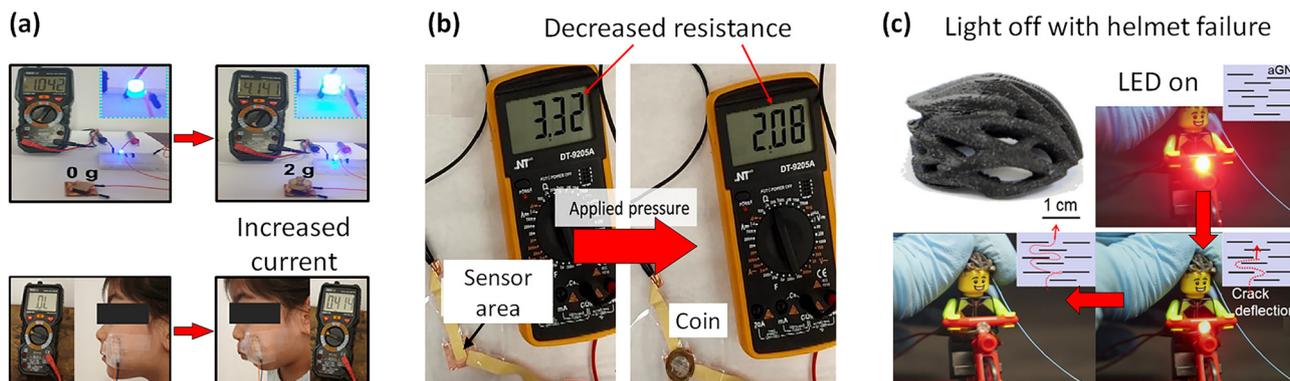
Fig. 9 Force sensing achieved with (a) a nacre-like scaffold made of graphene oxide, MXene, and silk fibroin, (b) a nacre-like material made of graphite and PDMS, and (c) a nacre-like smart helmet made of graphene nanosheets. Image (a) is adapted with permission from ref. 25. Copyright 2021 American Chemical Society. The images (b) and (c) are adapted from ref. 43 and 38.

after placing a coin on top of the sensor area with an ohmmeter (Fig. 9(b)). The graphite platelets moved closer together due to the weight of the coin, which decreased the material's overall electrical resistance and reflected in the readings on the ohmmeter (Fig. 9(b)). Meanwhile, due to the high platelet content, a pressure-sensing range of up to 300 kPa was successfully achieved.[43]

Besides force, damage can be sensed, as well. A nacre-like material able to self-report crack formation is made of graphene nanosheets (GN) ('bricks') and photocurable resin ('mortar'). The combination of photopolymerization-based 3D printing and electrical-assisted assembly was used in the fabrication process.[38] Prior to the printing process, 2 wt% GN in a vat of photocurable resin ('mortar') were electrically aligned to form the nacre-like architecture between opposing electrodes. A 3D nacre-like smart helmet with self-sensing capability was subsequently printed through the layer-by-layer printing process. The self-sensing capability of the material was demonstrated by attaching the helmet to an LED and monitoring the LED brightness. When a compression force was applied to the helmet, the formation of cracks caused the overall electrical resistance to increase, which caused the LED brightness to decrease (Fig. 9(c)). The material failed completely and caused the LED to turn off (Fig. 9c).[38]

3.3. Bioactivity

One of the classical challenges of using materials for biomedical applications, particularly when hard biomaterials are needed, is the fusion of bioactivity with mechanical properties. For instance, most synthetic bone grafts cannot simultaneously provide sufficient mechanical properties, bioactivity, and controlled biodegradability to promote bone tissue regeneration.[113] Although metals, such as titanium alloys, provide adequate mechanical properties to withstand cyclic loads resulting from daily physical activities, their bioactivity remains limited.[55,114] On the other hand, bio-ceramics, such as silica-based bone grafts, can supply sufficient bioactivity. However, their mechanical performance and range of applicability in load-bearing bones are constrained by their brittleness.[115,116]

Current biopolymers are also non-optimal materials for bone grafts, as they feature low stiffness and strength.[117] Therefore, the use of nacre-like materials as biomaterials provides an opportunity to combine the bioactivity, stiffness, and strength of bioceramic (or bioactive glasses) with the toughness of biopolymers and metals.

Various bioceramics, including silicate-based ceramic powder or platelets,[118] hydroxyapatite powder or platelets,[119] and graphene oxide,[120] have been considered as the 'bricks' to make bioactive nacre-like materials. For the 'mortar' phase, biopolymers such as chitosan have been used.[121] These bioactive nacre-like materials have been hard and therefore relevant to hard tissues of the body: mostly bones. They have been so far used for two types of bone defects: surface and long defects. An example is a biomembrane made for bone surface defects (Fig. 10(a)). The fabrication process involves sedimentation and evaporation, with graphene oxide (GO) constituting the 'bricks' and chitosan (CS)–calcium silicate (CaSi) nanowires forming the 'mortar' phase. Subsequently, a porous layer was constructed onto the nacre-like layer by spray-coating and freeze-drying a mixture of the CS–GO–CaSi to enhance osteoblast adhesion. GO was employed as the 'bricks' because of its strength and biocompatibility. CS and CaSi were selected as the 'mortar' due to their biodegradability and antibacterial properties.[122] The bioactivity of the prepared membrane was subsequently assessed *in vitro*, where 90% human mesenchymal stem cell attachment efficiency was achieved after 6 hours of culture, and cells remained viable. The results show that the material prevents the surrounding fibroblasts and epithelial cells from influencing bone formation.[73] However, further *in vivo* and clinical studies are required to confirm the clinical efficacy of the nacre-like biomembrane.

Nacre-like materials have been used for long bone defects, as well. For example, a cylinder-shaped bone graft was made by coiling nacre-like biofilm made of GO ('bricks') and CS ('mortar') (Fig. 10(b)).[26] The biofilm was assembled through vacuum filtration, and 20 vol% hydroxyapatite (HA) was added to the film to increase the bioactivity of the material further. In another study, to eliminate the need for coiling, Akermanite
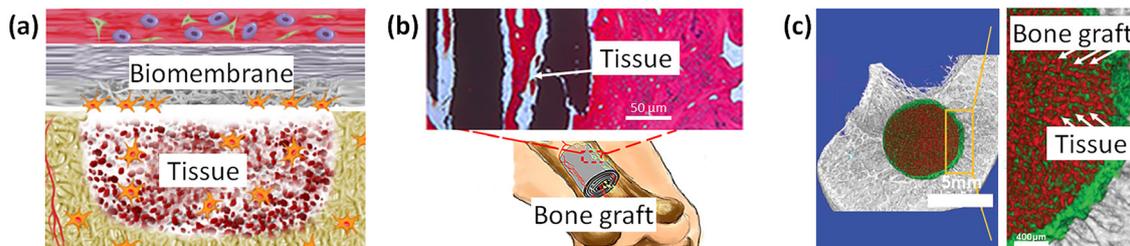
Fig. 10 Bioactivity achieved with (a) the CS–GO–CaSi biomembrane, (b) the coiled GO-CS-HA synthetic bone graft, and (c) the synthetic bone graft with nacre-like architecture (red: materials, green: new bone). Images are reproduced from ref. 73, 26, and 123 with permissions respectively from Elsevier Inc, copyright 2019, Elsevier Ltd, copyright 2020, and WILEY-VCH Verlag GmbH & Co. KGaA, Weinheim, copyright 2020.

(AKT), a silicate-based bioceramic,[124,125] were assembled into a 3D material using the bidirectional freeze-casting technique (Fig. 10(c)).[123] The lamellar architecture resulting from freeze-casting was subsequently heat-treated and infiltrated with a kind of biopolymer commonly used for restoring teeth fracture (Bis-GMA/TEGDMA) to form the nacre-like bone graft. Both studies subsequently assessed the bioactivity of the made bone graft *in vivo* by implanting it into the femoral defect of a rabbit.[26,123] After 12 weeks of implantation, 11.5% ± 1.1% of newly formed bone was found in bone grafts made of bidirectional freeze-casting according to histomorphometric assay, compared with the control group (3.62% ± 1.37%).[123] The enhanced bone formation can be attributed to the interconnected lamellar nacre-like architecture that provides a conducive environment for accelerated bone growth (Fig. 10(c)).[126] Several other studies have also used nacre-like materials made of other bioceramic and through other fabrication methods for bone grafts.[127,128]

3.4. Transparency

Transparency refers to the ability of a material to transmit light without any scattering, absorption, or distortion. Today, transparent materials find applications in various industries ranging from the screens of electronic devices and windshields of cars[129–131] to critical components of state-of-the-art chemical analysis devices.[132] The most used transparent materials include silica-based glasses or transparent polymers such as polycarbonate-based materials.[133] Silica-based glasses are prone to shatter into pieces upon significant impact, while transparent polymers lack adequate wear resistance and strength to be used as structural components.[134,135] Although fabrication techniques such as thermal-tempering and lamination with soft polymeric layers have been used to increase the impact resistance of glass materials, the range of toughening mechanisms implemented in these materials is limited compared to natural materials such as nacre.[136–138] Thus, incorporating nacre-like architecture into the fabrication of transparent materials could be developed as the next generation of laminated glass used in windshields and transparent armour.

Using laser engraving to fabricate nacre-like glassy materials with excellent shape and alignment control for building blocks ranging from 1 mm to 10 mm has been discussed in the previous section.[10] The light transmittance level of the resulting glass composite reached 70–80% across the visible light spectrum.[10] However, laser engraving glass plates to form smaller building blocks is currently challenging. To achieve nacre-like transparent materials with smaller building blocks, layered double hydroxide (LDH) platelets of $Co–NO_3$ and $Co–Al–CO_3$ have been made to be the 'bricks' in a nacre-like composite with chitosan.[80] The platelets were synthesized according to the previously published method and assembled onto a glass substrate through the dip-coating technique. A chitosan layer was spin-coated onto the surface to serve as the 'mortar' phrase of the film. The process was repeated until a complete nacre-like film was achieved. Light transmittance experiments indicated that the $Co–NO_3$–chitosan film only allowed visible light between 400 nm to 600 nm to pass, whereas $Co–Al–CO_3$–chitosan showed 40–70% transmittance levels across the entire spectrum of visible light (400 nm to 800 nm) (Fig. 11a).[80]

To extend the application beyond transparent films, a nacre-like glass 3D scaffold was achieved by assembling high aspect ratio silica-based glass microplatelets ('bricks') through vacuum filtration.[94] Subsequent compression and sintering processes were used to improve the alignment of the platelets and further consolidate the architecture. A mixture of PMMA and phenanthrene (PHN) ('mortar') was finally infiltrated into the architecture and formed a nacre-like scaffold with optical transparency (Fig. 11(b)). The combination of PMMA and PHN was selected due to the PHN's ability to modify the refractive index of PMMA to match that of glass. Light transmittance experiments showed 45–55% light transmittance across the entire visible light spectrum, which is lower than that achieved by transparent nacre-like film. The reason for this difference can be attributed to the presence of small pores between the soft 'mortar' phase and hard 'bricks' phase. These pores potentially caused light scattering and reduced the overall transmittance of the material.[94]

The transparency of the material was further enhanced by increasing the compactness of the material using centrifugation, which also resulted in good alignment of the used silica-based glass platelets.[11] During the fabrication process, silica-glass platelets, poly(methyl methacrylate) (PMMA), and PHN molecules were mixed together before centrifuging at 2000 g. The glass platelets stacked on top of each other due to the centrifugation force to form the 'bricks' part of the architecture
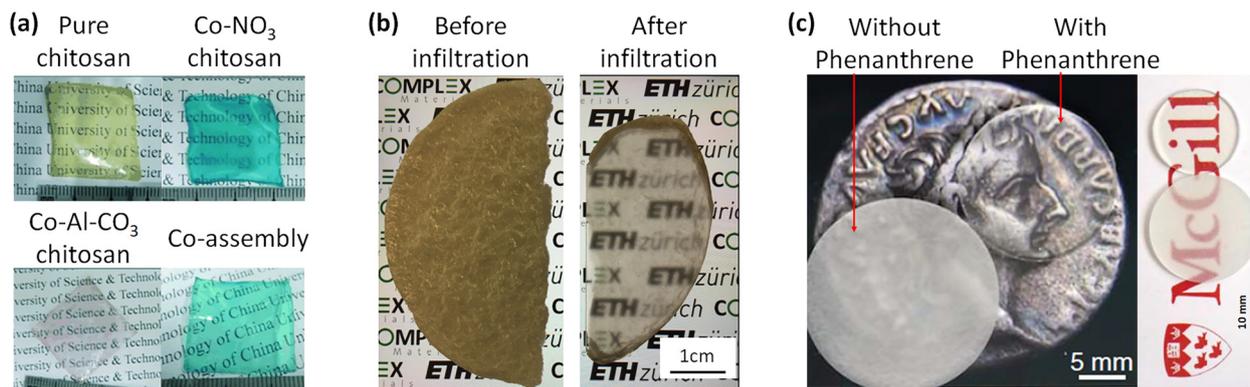
Fig. 11 Transparency achieved with (a) the nacre-like film made of layered double hydroxide and chitosan, (b) the nacre-like scaffold made of glass microplatelets and PMMA/PHN, and (c) the nacre-like scaffold made of glass flakes and PMMA/PHN through centrifugation. Images (a) and (c) are reproduced from ref. 80 and 11 with permissions respectively from WILEY-VCH Verlag GmbH & Co. KGaA, Weinheim, copyright 2010, and the American Association for the Advancement of Science, copyright 2021. Image (b) is adapted from ref. 94.

at the bottom of the mould, while polymerization of PMMA was achieved *via* a series of heat treatments and formed the 'mortar' part of the nacre-like architecture. Further light transmittance tests showed 80% to 90% transmittance across the visible light spectrum (400 nm to 800 nm), which is nearly twice the transparent material developed through vacuum filtration (Fig. 11(c)).[11]

3.5. Heat conductivity and resistance

Heat resistance is critical for applications such as aerospace[139,140] and protective systems, as the internal components need to be protected from external heat to prevent thermal damage, degradation, and failure. Nacre-like structures can be incorporated into heat-resistant materials by using building blocks with sufficient heat-resistant properties. On the other hand, thermal conductivity is also required in applications such as electronic packaging, where unwanted internal heat must be transferred to the outside to maintain performance and extend the service life of electrical components.[75]

To enable the successful usage of nacre-like architecture, ceramics like boron nitride (BN) and alumina platelets with high heat conductivity have been used.[141–143] For example, boron nitride platelets were employed as the 'bricks' and assembled into nacre-like materials through solid-phase extrusion with ultra-high molecular weight polyethylene (UHMWPE) lamellae as the 'mortar' phase.[27] The well-oriented structure enabled by nacre-like architecture concomitantly improved the heat conduction of the material: the heat conductivity of the nacre-like material was almost 4 times higher (12.42 W mK^{-1}) than the materials made of high-pressure moulding. Heat transfer could be seen as the migration of phonons from the hot side to the cold side. Therefore, as the heat transfer rate of the BN platelets is much higher than the UHMWPE 'mortar' phase, the closely connected BN platelets provided an unimpeded pathway for heat transfer. Consequently, as phonons travel much faster along the basal plane than through the prismatic plane of the nano-platelets, the heat conduction rate in the in-plane direction is much faster than in the through-plane direction (Fig. 12(a)). When nacre-like materials and materials made of high-pressure moulding were both tested under an infrared camera, the heat transfer rate was visually displayed. The results indicated the fastest heat transfer rate for nacre-like materials in the in-plane direction (Fig. 12(a)).[27]

In addition to ceramics, metals including nickel,[63] aluminium,[97] iron,[71] and amorphous metal alloys such as zirconia-based bulk-metallic glass[13] have been incorporated into nacre-like material as the 'mortar' phase to provide
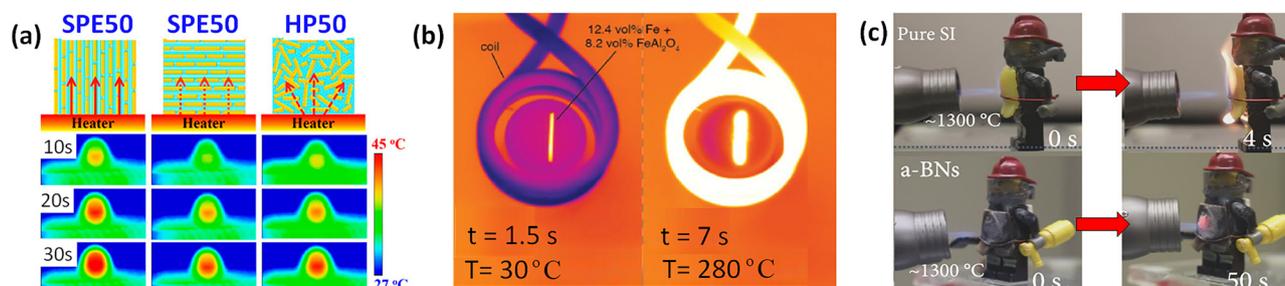

Fig. 12 Heat conductivity and resistance achieved with (a) nacre-like composite made of boron nitride platelets and UHMWPE, (b) nacre-like architectures made of Fe-coated alumina platelets, and (c) 3D nacre-like material made of boron nitride platelets. Image (a) is adapted with permission from ref. 27. Copyright 2018 American Chemical Society. Images (b) and (c) are adapted from ref. 42 and 71 respectively.

thermal functionality. For example, iron-coated alumina platelets have been used to assemble into nacre-like materials through magnetic-assisted slip-casting.[71] During the fabrication process, a layer of iron acetylacetonate precursor was initially deposited onto the platelet's surface and transformed into an iron coating after a series of heat treatments. Finally, all the platelets were aligned into the layered nacre-like architecture using magnetic-assisted slip-casting followed by spark plasma sintering. The thermal functionality of the material was further evidenced when subjecting the material to induction heating, where it only took as little as 5.5 s for the material's temperature to increase from 30 to 280 °C (Fig. 12(b)).[71]

To implement heat resistance, using high-temperature stable 'brick' materials such as montmorillonite (MMT) platelets,[76] MXene nanosheets,[77,78] or BN platelets[144,145] is perhaps the simplest and most effective way. As mentioned in Section 2, a custom-built 3D printer recently achieved a nacre-like architecture consisting of 55 wt% boron nitride (BN) nanoplatelets through doctor-blading.[42] The heat resistance of the material was further tested by exposing the material to the flame of a torch fire (around 1300 °C), where the nacre-like material did not incinerate after 50 seconds of exposure (Fig. 12(c)). After the heat resistance test, no cracks or expansions were seen at the surface of the materials, indicating the thermal shielding capability. Moreover, when a thermocouple was placed behind the materials, after 25 seconds of exposure to the torch fire, the temperature went to 193 °C, which is around 85% (1107 °C) lower than that achieved by the material made of pure printing resin.[42]

3.6. Electromagnetic interference shielding

Electronic devices are getting smarter and smaller, and therefore respectively more useful and easier to use. However, the challenge is that these devices emit electromagnetic interference (EMI)[146] waves and cause detrimental effects on the performance of the device itself and the surrounding devices.[147,148] Thus, the question of how the migration of and shielding from undesired EMI can be achieved has become an important field in material science. MXene, a class of two-dimensional (2D) transition metal carbides and/or nitrides, is highly electrically conductive and assumes a leading role in EMI shielding applications.[149,150] However, freestanding MXene nanosheets suffer from poor mechanical properties due to weak interplatelet interactions between adjacent layers.[151,152] Thus, using the nacre-like architecture with MXene functional building blocks to achieve mechanically stable materials with enhanced EMI shielding functionality is an active research field.

Fortunately, MXene nanosheets are terminated with numerous functional groups (T_x) such as –OH, =O, and –F, allowing them to readily bind with a variety of polymers and nanofibers through hydrogen bonding. So, a good binding can be achieved when these materials are arranged in a nacre-like architecture.[153] As an illustration, cellulose nanofibers (CNF) have been combined with $Ti_3C_2T_x$ MXene nanosheets to make nacre-like films with EMI shielding. CNFs, known for their mechanical strength and flexibility, were extracted from dried garlic husks.[154,155] The MXene ('bricks') and CNFs ('mortar') were assembled into a nacre-like film through vacuum filtration. The EMI shielding effectiveness (EMI SE_T) is measured by comparing the intensity of the electromagnetic radiation before and after the materials are placed inside the waveguide at a given frequency range. In the case of nacre-like film containing 80 wt% MXene nanosheets with a thickness of 74 μm, an EMI SE_T up to 25 dB was achieved in the frequency between 8 to 12.4 GHz (X-band).[74] More recently, an EMI nacre-like shield was made by doctor-blading a mixture of $Ti_3C_2T_x$ MXene nanosheets ('bricks') and aramid fibres ('mortar') onto a glass plate. Using doctor-blading, the nacre-like film with a large area = 600 cm² was made.[79] The EMI shielding effectiveness test showed the nacre-like film with 80 wt% MXene nanosheets to feature an EMI SE_T of 48 dB in the X-band.[79]

In addition to achieving high EMI shielding effectiveness, ensuring flame retardancy is a vital consideration for EMI shielding materials. This is particularly critical for preventing fire hazards resulting from accidental battery leakage or wire aging in electronic devices.[156,157] To address this requirement, researchers coated a MXene sheet with nacre-like films made of montmorillonite (MMT) platelet as 'bricks', and calcium ion-crosslinked sodium alginate (CSA) as mortar.[29] The MMT was selected due to its flame retardancy properties,[76,158] and CSA was selected for its mechanical characteristics.[159] The flame retardancy of the material was assessed by exposing the film to an alcohol lamp flame for 3 minutes, where the film remained inflammable throughout the entire heating process. Finally, the EMI shielding effectiveness of the film was found to be at the same level as pure MXene sheets (EMI SE_T = 50.01 dB) in the X-band. Meanwhile, its strength and toughness were respectively almost 20 times and 6 times higher than the pure MXene sheets.[29]

4. Outlook

Since the initial development of nacre-like materials around three decades ago,[160] various fabrication techniques such as 3D printing, freeze-casting, mixing/coating-assembling, and laser engraving have been developed. These nacre-like materials have taken different forms, from thin films to plates and complex 3D shapes, and have shown promising combinations of physical, chemical, and biological properties. However, challenges remain in the high throughput fabrication of these materials made of nm- to μm-sized building blocks and forming them into complex shapes in sizes sufficiently large for practical applications.

Recent advances in 3D printing procedures using both photopolymerization,[161,162] and extrusion-based[163] techniques promise complete control over the geometry and the assembly of the building blocks with minimum feature size printable in the 50 to 100 μm range. Combining these techniques with

recent advances in 4D printing of ceramics and composites shows promising pathways to obtain complex shapes.[164–167] For example, we have recently shown that the shape change behaviour can be achieved through anisotropic shrinkage caused by heterogeneous particle concentrations within the ceramic green body during the ceramic sintering process. Introducing heterogeneous green body compositions to an architectured green body can lead to nacre-like (and other) architectured ceramics with complex shapes: a 2D flat green body with a hexagonal architecture and heterogeneous concentration of particles can turn into a cylindrical-shaped nacre-like component during the ceramic sintering process – a shape useful for bone grafting.

On the other hand, the advance of modelling tools such as machine learning,[168] finite element analysis,[169] discrete elements,[170] and analytical models[171] promises pathways to identify new sets of shapes, other than the current flat and bowtie platelets that have the potential to break the trade-off between toughness and strength in different loading conditions. These modelling techniques can also answer questions on how to arrange these building blocks in complex shapes required for many applications. For example, orthopaedic applications need components duplicating the complex shapes of bones. Protective systems should match the complex shapes of the underlying components or tissues. Besides modelling techniques, advanced characterization techniques such as testing under *in situ* μ-computed tomography (μCT) promise to reveal new architecture-performance relationships, which can be used to further optimize the block shapes and, in turn, material performance.

A further promising direction is to use engineering mechanisms and elements, such as linkages, to alter the internal architecture and, consequently, the mechanical properties of nacre-like materials *in situ*. Machine elements have been recently used to reprogram the stiffness and shape of mechanical metamaterials.[172] Similar ideas might be implemented in nacre-like materials to alter their architectures drastically and continuously (*e.g.*, interlocking angle) and, in turn, reprogram their behaviour (*e.g.*, stiffness) *in situ*. Such adaptations can be made reversible over numerous cycles, with low energy absorption, inducing only low mechanical stresses and strains.[173] Live materials containing active microorganisms that can adapt to the environment and repair themselves are usually soft.[174] Using these materials in combination with stiffer building blocks arranged, for example, in nacre-like architecture, would likely improve their stiffness and strength, while maintaining their damage-sensing and self-repair capabilities. Such progress necessitates ethical and regulatory considerations.

Our current review highlights that nacre-like materials are powerful entities for combining stiffness, strength, toughness as well as other functionalities. Resolving the current issues related to making large components with small blocks, high throughput fabrication, and forming the material into complex shapes facilitates translation to industry, which is still a challenge for bioinspired materials, including nacre-like composites.

Author contributions

Conflicts of interest

The authors declare no competing interests.

Acknowledgements

References

1 R. O. Ritchie, *Nat. Mater.*, 2011, **10**, 817–822.
2 M. A. Meyers, P.-Y. Chen, A. Y.-M. Lin and Y. Seki, *Prog. Mater. Sci.*, 2008, **53**, 1–206.
3 F. Barthelat, Z. Yin and M. J. Buehler, *Nat. Rev. Mater.*, 2016, **1**, 1–16.
4 M. Mirkhalaf and H. Zreiqat, *JOM*, 2020, **72**, 1458–1476.
5 N. San Ha and G. Lu, *Composites, Part B*, 2020, **181**, 107496.
6 F. Barthelat, H. Tang, P. Zavattieri, C.-M. Li and H. Espinosa, *J. Mech. Phys. Solids*, 2007, **55**, 306–337.
7 U. G. Wegst, H. Bai, E. Saiz, A. P. Tomsia and R. O. Ritchie, *Nat. Mater.*, 2015, **14**, 23–36.
8 L. Bédouet, A. Marie, L. Dubost, J. Péduzzi, D. Duplat, S. Berland, M. Puisségur, H. Boulzaguet, M. Rousseau and C. Milet, *Mar. Biotechnol.*, 2007, **9**, 638–649.
9 F. Bouville, *J. Mater. Res.*, 2020, **35**, 1076–1094.
10 Z. Yin, F. Hannard and F. Barthelat, *Science*, 2019, **364**, 1260–1263.
11 A. Amini, A. Khavari, F. Barthelat and A. J. Ehrlicher, *Science*, 2021, **373**, 1229–1234.
12 T. Magrini, S. Moser, M. Fellner, A. Lauria, F. Bouville and A. R. Studart, *Adv. Funct. Mater.*, 2020, **30**, 2002149.
13 A. Wat, J. I. Lee, C. W. Ryu, B. Gludovatz, J. Kim, A. P. Tomsia, T. Ishikawa, J. Schmitz, A. Meyer and M. Alfreider, *Nat. Commun.*, 2019, **10**(1), 961.
14 J. Bauer, A. Schroer, R. Schwaiger and O. Kraft, *Nat. Mater.*, 2016, **15**, 438.
15 H. Gao, B. Ji, I. L. Jäger, E. Arzt and P. Fratzl, *Proc. Natl. Acad. Sci. U. S. A.*, 2003, **100**, 5597–5600.

16 M. Mirkhalaf, T. Zhou and F. Barthelat, *Proc. Natl. Acad. Sci. U. S. A.*, 2018, **115**, 9128–9133.

17 M. Mirkhalaf, A. Sunesara, B. Ashrafi and F. Barthelat, *Int. J. Solids Struct.*, 2019, **158**, 52–65.

18 P. Fratzl, O. Kolednik, F. D. Fischer and M. N. Dean, *Chem. Soc. Rev.*, 2016, **45**, 252–267.

19 W. Huang, D. Restrepo, J. Y. Jung, F. Y. Su, Z. Liu, R. O. Ritchie, J. McKittrick, P. Zavattieri and D. Kisailus, *Adv. Mater.*, 2019, **31**, 1901561.

20 W. Zhang, J. Xu and T. Yu, *Eng. Struct.*, 2022, **265**, 114490.

21 H. Zhao and L. Guo, *Adv. Mater.*, 2017, **29**, 1702903.

22 A. R. Studart, *Chem. Soc. Rev.*, 2016, **45**, 359–376.

23 I. Corni, T. Harvey, J. Wharton, K. Stokes, F. Walsh and R. Wood, *Bioinspiration Biomimetics*, 2012, **7**, 031001.

24 V. Restrepo and R. V. Martinez, *Mater. Des.*, 2021, **205**, 109691.

25 M. Bandar Abadi, R. Weissing, M. Wilhelm, Y. Demidov, J. Auer, S. Ghazanfari, B. Anasori, S. Mathur and H. Maleki, *ACS Appl. Mater. Interfaces*, 2021, **13**, 34996–35007.

26 C. Feng, J. Xue, X. Yu, D. Zhai, R. Lin, M. Zhang, L. Xia, X. Wang, Q. Yao and J. Chang, *Acta Biomater.*, 2021, **119**, 419–431.

27 Y.-F. Huang, Z.-G. Wang, H.-M. Yin, J.-Z. Xu, Y. Chen, J. Lei, L. Zhu, F. Gong and Z.-M. Li, *ACS Appl. Nano Mater.*, 2018, **1**(7), 3312–3320.

28 S. Liu, S. Wang, M. Sang, J. Zhou, J. Zhang, S. Xuan and X. Gong, *ACS Nano*, 2022, **16**, 19067–19086.

29 Y. Zhang, W. Cheng, W. Tian, J. Lu, L. Song, K. M. Liew, B. Wang and Y. Hu, *ACS Appl. Mater. Interfaces*, 2020, **12**, 6371–6382.

30 M. Mirkhalaf, A. K. Dastjerdi and F. Barthelat, *Nat. Commun.*, 2014, **5**, 1–9.

31 E. Munch, E. Saiz, A. P. Tomsia and S. Deville, *J. Am. Ceram. Soc.*, 2009, **92**, 1534–1539.

32 M. Mirkhalaf and F. Barthelat, *Extreme Mech. Lett.*, 2017, **11**, 1–7.

33 J. R. Raney, B. G. Compton, J. Mueller, T. J. Ober, K. Shea and J. A. Lewis, *Proc. Natl. Acad. Sci. U. S. A.*, 2018, **115**, 1198–1203.

34 J. J. Martin, B. E. Fiore and R. M. Erb, *Nat. Commun.*, 2015, **6**, 8641.

35 A.-K. Hofer, I. Kraleva and R. Bermejo, *Open Ceram.*, 2021, **5**, 100085.

36 X. Wu, Z. Zhang, D. Ma, X. Lu, Z. Chen, Y. Gao and C. Xu, *Ceram. Int.*, 2022, **48**, 13134–13143.

37 E. Feilden, C. Ferraro, Q. Zhang, E. García-Tuñón, E. D'Elia, F. Giuliani, L. Vandeperre and E. Saiz, *Sci. Rep.*, 2017, **7**, 13759.

38 Y. Yang, X. Li, M. Chu, H. Sun, J. Jin, K. Yu, Q. Wang, Q. Zhou and Y. Chen, *Sci. Adv.*, 2019, **5**, eaau9490.

39 D. Kokkinis, M. Schaffner and A. R. Studart, *Nat. Commun.*, 2015, **6**, 8643.

40 A. Walther, I. Bjurhager, J. M. Malho, J. Pere, J. Ruokolainen, L. A. Berglund and O. Ikkala, *Nano Lett.*, 2010, **10**, 2742–2748.

41 M. Mirkhalaf and F. Barthelat, *J. Mech. Behav. Biomed. Mater.*, 2016, **56**, 23–33.

42 Y. Yang, Z. Wang, Q. He, X. Li, G. Lu, L. Jiang, Y. Zeng, B. Bethers, J. Jin and S. Lin, *Research*, 2022, **2022**, 9840574.

43 W. C. Liu, V. H. Y. Chou, R. P. Behera and H. Le Ferrand, *Nat. Commun.*, 2022, **13**, 5015.

44 S. Mahmood Khan, Z. Deng, T. Yang and L. Li, *Adv. Eng. Mater.*, 2022, **24**, 2101009.

45 B. Raju, S. Hiremath and D. R. Mahapatra, *Compos. Struct.*, 2018, **204**, 607–619.

46 J. Wettlaufer, M. G. Worster and H. E. Huppert, *J. Fluid Mech.*, 1997, **344**, 291–316.

47 S. Deville, E. Saiz, R. K. Nalla and A. P. Tomsia, *Science*, 2006, **311**, 515–518.

48 E. Munch, M. E. Launey, D. H. Alsem, E. Saiz, A. P. Tomsia and R. O. Ritchie, *Science*, 2008, **322**, 1516–1520.

49 G. Du, A. Mao, J. Yu, J. Hou, N. Zhao, J. Han, Q. Zhao, W. Gao, T. Xie and H. Bai, *Nat. Commun.*, 2019, **10**.

50 M. J. Garnier and D. C. Dunand, *Mater. Sci. Eng., A*, 2019, **743**, 190–196.

51 N. Guo, P. Shen, R.-F. Guo and Q.-C. Jiang, *Mater. Sci. Eng., A*, 2019, **748**, 286–293.

52 T. Waschkies, R. Oberacker and M. J. Hoffmann, *J. Am. Ceram. Soc.*, 2009, **92**, S79–S84.

53 M. E. Launey, E. Munch, D. H. Alsem, E. Saiz, A. P. Tomsia and R. O. Ritchie, *J. R. Soc., Interface*, 2010, **7**, 741–753.

54 H. Bai, Y. Chen, B. Delattre, A. P. Tomsia and R. O. Ritchie, *Sci. Adv.*, 2015, **1**, e1500849.

55 F. Bouville, E. Maire, S. Meille, B. Van de Moortèle, A. J. Stevenson and S. Deville, *Nat. Mater.*, 2014, **13**, 508–514.

56 N. Zhao, M. Li, H. Gong and H. Bai, *Sci. Adv.*, 2020, **6**, eabb4712.

57 R.-F. Guo, Z.-J. Hu, A. Shaga and P. Shen, *Composites, Part A*, 2023, **165**, 107347.

58 K. L. Scotti, L. G. Kearney, J. Burns, M. Ocana, L. Duros, A. Shelhamer and D. C. Dunand, *J. Eur. Ceram. Soc.*, 2019, **39**, 3180–3193.

59 A. Lasalle, C. Guizard, E. Maire, J. Adrien and S. Deville, *Acta Mater.*, 2012, **60**, 4594–4603.

60 Y.-L. Li, R.-F. Guo, Z.-J. Hu and P. Shen, *Mater. Des.*, 2021, **204**, 109668.

61 H. Le Ferrand, F. Bouville, T. P. Niebel and A. R. Studart, *Nat. Mater.*, 2015, **14**, 1172–1179.

62 M. Cerbelaud, M. Muñoz, F. Rossignol and A. Videcoq, *Langmuir*, 2020, **36**, 3315–3322.

63 A. Wat, C. Ferraro, X. Deng, A. Sweet, A. P. Tomsia, E. Saiz and R. O. Ritchie, *Small*, 2019, **15**, 1900573.

64 D. Ji and J. Kim, *ACS Nano*, 2019, **13**, 2773–2785.

65 Y. Q. Li, T. Yu, T. Y. Yang, L. X. Zheng and K. Liao, *Adv. Mater.*, 2012, **24**, 3426–3431.

66 W. Cui, M. Li, J. Liu, B. Wang, C. Zhang, L. Jiang and Q. Cheng, *ACS Nano*, 2014, **8**, 9511–9517.

67 L. Medina, Y. Nishiyama, K. Daicho, T. Saito, M. Yan and L. A. Berglund, *Macromolecules*, 2019, **52**, 3131–3140.

68 P. Laaksonen, A. Walther, J. M. Malho, M. Kainlauri, O. Ikkala and M. B. Linder, *Angew. Chem., Int. Ed.*, 2011, **50**, 8688–8691.

69 C.-A. Wang, B. Long, W. Lin, Y. Huang and J. Sun, *J. Mater. Res.*, 2008, **23**, 1706–1712.

70 T. Guo, L. Heng, M. Wang, J. Wang and L. Jiang, *Adv. Mater.*, 2016, **28**, 8505–8510.

71 E. Poloni, F. Bouville, C. H. Dreimol, T. P. Niebel, T. Weber, A. R. Biedermann, A. M. Hirt and A. R. Studart, *Sci. Rep.*, 2021, **11**.

72 H. Zhao, Z. Yang and L. Guo, *NPG Asia Mater.*, 2018, **10**, 1–22.

73 K.-R. Zhang, H.-L. Gao, X.-F. Pan, P. Zhou, X. Xing, R. Xu, Z. Pan, S. Wang, Y. Zhu and B. Hu, *Matter*, 2019, **1**, 770–781.

74 W.-T. Cao, F.-F. Chen, Y.-J. Zhu, Y.-G. Zhang, Y.-Y. Jiang, M.-G. Ma and F. Chen, *ACS Nano*, 2018, **12**, 4583–4593.

75 X. Zeng, L. Ye, S. Yu, H. Li, R. Sun, J. Xu and C.-P. Wong, *Nanoscale*, 2015, **7**, 6774–6781.

76 P. Ming, Z. Song, S. Gong, Y. Zhang, J. Duan, Q. Zhang, L. Jiang and Q. Cheng, *J. Mater. Chem. A*, 2015, **3**, 21194–21200.

77 E. Jiao, K. Wu, Y. Liu, M. Lu, Z. Hu, B. Chen, J. Shi and M. Lu, *Composites, Part A*, 2021, **146**, 106417.

78 Y. Zhan, B. Nan, Y. Liu, E. Jiao, J. Shi, M. Lu and K. Wu, *Chem. Eng. J.*, 2021, **421**, 129733.

79 J. Wang, X. Ma, J. Zhou, F. Du and C. Teng, *ACS Nano*, 2022, **16**, 6700–6711.

80 H. B. Yao, H. Y. Fang, Z. H. Tan, L. H. Wu and S. H. Yu, *Angew. Chem.*, 2010, **122**, 2186–2191.

81 G. M. Whitesides and B. Grzybowski, *Science*, 2002, **295**, 2418–2421.

82 P. I. Pelissari, F. Bouville, V. C. Pandolfelli, D. Carnelli, F. Giuliani, A. P. Luz, E. Saiz and A. R. Studart, *J. Eur. Ceram. Soc.*, 2018, **38**, 2186–2193.

83 L. J. Bonderer, K. Feldman and L. J. Gauckler, *Compos. Sci. Technol.*, 2010, **70**, 1958–1965.

84 S. Sapasakulvanit, X. Y. Chan and H. Le Ferrand, *Bioinspiration Biomimetics*, 2023, **18**, 046009.

85 R. P. Wilkerson, B. Gludovatz, J. Watts, A. P. Tomsia, G. E. Hilmas and R. O. Ritchie, *Adv. Mater.*, 2016, **28**, 10061–10067.

86 Z. Xu, J. Huang, C. Zhang, S. Daryadel, A. Behroozfar, B. McWilliams, B. Boesl, A. Agarwal and M. Minary-Jolandan, *Adv. Eng. Mater.*, 2018, **20**, 1700782.

87 D. Mereib, U. Seu, C. Chung, M. Zakhour, M. Nakhl, N. Tessier-Doyen, J.-L. Bobet and J.-F. Silvain, *J. Mater. Sci.*, 2018, **53**, 7857–7868.

88 I. A. Malik and F. Barthelat, *Int. J. Solids Struct.*, 2016, **97**, 389–399.

89 H. Yazdani Sarvestani, I. Esmail, Z. Katz, S. Jain, J. Sa, D. Backman and B. Ashrafi, *Sci. Rep.*, 2022, **12**, 17330.

90 M. Mirkhalaf, J. Tanguay and F. Barthelat, *Extreme Mech. Lett.*, 2016, **7**, 104–113.

91 S. M. M. Valashani and F. Barthelat, *Bioinspiration Biomimetics*, 2015, **10**, 026005.

92 Z. Yin and F. Barthelat, *Bioinspiration Biomimetics*, 2021, **16**, 026020.

93 S. M. M. Valashani, C. J. Barrett and F. Barthelat, *RSC Adv.*, 2015, **5**, 4780–4787.

94 T. Magrini, F. Bouville, A. Lauria, H. Le Ferrand, T. P. Niebel and A. R. Studart, *Nat. Commun.*, 2019, **10**, 2794.

95 H.-L. Gao, S.-M. Chen, L.-B. Mao, Z.-Q. Song, H.-B. Yao, H. Cölfen, X.-S. Luo, F. Zhang, Z. Pan and Y.-F. Meng, *Nat. Commun.*, 2017, **8**, 287.

96 M. Grossman, F. Bouville, F. Erni, K. Masania, R. Libanori and A. R. Studart, *Adv. Mater.*, 2017, **29**, 1605039.

97 C. Ferraro, S. Meille, J. Réthoré, N. Ni, J. Chevalier and E. Saiz, *Acta Mater.*, 2018, **144**, 202–215.

98 R. P. Wilkerson, B. Gludovatz, J. Watts, A. P. Tomsia, G. E. Hilmas and R. O. Ritchie, *Acta Mater.*, 2018, **148**, 147–155.

99 H. Y. Sarvestani, M. Mirkhalaf, A. Akbarzadeh, D. Backman, M. Genest and B. Ashrafi, *Mater. Des.*, 2019, **167**, 107627.

100 Q. Zhao, H. J. Qi and T. Xie, *Prog. Polym. Sci.*, 2015, **49**, 79–120.

101 B. Zhu, N. Jasinski, A. Benitez, M. Noack, D. Park, A. S. Goldmann, C. Barner-Kowollik and A. Walther, *Angew. Chem., Int. Ed.*, 2015, **54**, 8653–8657.

102 P. Cordier, F. Tournilhac, C. Soulié-Ziakovic and L. Leibler, *Nature*, 2008, **451**, 977–980.

103 G. M. van Gemert, J. W. Peeters, S. H. Söntjens, H. M. Janssen and A. W. Bosman, *Macromol. Chem. Phys.*, 2012, **213**, 234–242.

104 M. Burnworth, L. Tang, J. R. Kumpfer, A. J. Duncan, F. L. Beyer, G. L. Fiore, S. J. Rowan and C. Weder, *Nature*, 2011, **472**, 334–337.

105 B. Zhu, M. Noack, R. Merindol, C. Barner-Kowollik and A. Walther, *Nano Lett.*, 2016, **16**, 5176–5182.

106 W. P. Appel, G. Portale, E. Wisse, P. Y. Dankers and E. Meijer, *Macromolecules*, 2011, **44**, 6776–6784.

107 M. Hutin, E. Burakowska-Meise, W. P. Appel, P. Y. Dankers and E. Meijer, *Macromolecules*, 2013, **46**, 8528–8537.

108 P. Das, J.-M. Malho, K. Rahimi, F. H. Schacher, B. Wang, D. E. Demco and A. Walther, *Nat. Commun.*, 2015, **6**, 5967.

109 J. Vaicekauskaite, P. Mazurek, S. Vudayagiri and A. L. Skov, *J. Mater. Chem. C*, 2020, **8**, 1273–1279.

110 D. Balageas, C.-P. Fritzen and A. Güemes, *Structural health monitoring*, John Wiley & Sons, 2010.

111 J. P. Lynch and K. J. Loh, *Shock Vib. Dig.*, 2006, **38**, 91–130.

112 J. M. Brownjohn, *Philos. Trans. R. Soc., A*, 2007, **365**, 589–622.

113 O. Faour, R. Dimitriou, C. A. Cousins and P. V. Giannoudis, *Injury*, 2011, **42**, S87–S90.

114 K. Prasad, O. Bazaka, M. Chua, M. Rochford, L. Fedrick, J. Spoor, R. Symes, M. Tieppo, C. Collins and A. Cao, *Materials*, 2017, **10**, 884.

115 G. Ryan, A. Pandit and D. P. Apatsidis, *Biomaterials*, 2006, **27**, 2651–2670.

116 S. Dorozhkin, *J. Ceram. Sci. Technol.*, 2018, **9**, 353–370.

117 T. Kokubo, H.-M. Kim and M. Kawashita, *Biomaterials*, 2003, **24**, 2161–2175.

118 D. Arcos and M. Vallet-Regí, *Acta Biomater.*, 2010, **6**, 2874–2888.

119 W. Suchanek and M. Yoshimura, *J. Mater. Res.*, 1998, **13**, 94–117.

120 D. Ege, A. R. Kamali and A. R. Boccaccini, *Adv. Eng. Mater.*, 2017, **19**, 1700627.

121 F. Croisier and C. Jérôme, *Eur. Polym. J.*, 2013, **49**, 780–792.

122 A. Schlegel, H. Möhler, F. Busch and A. Mehl, *Biomaterials*, 1997, **18**, 535–538.

123 T. Li, B. Ma, J. Xue, D. Zhai, P. Zhao, J. Chang and C. Wu, *Adv. Healthcare Mater.*, 2020, **9**, 1901211.

124 Y. Huang, C. Wu, X. Zhang, J. Chang and K. Dai, *Acta Biomater.*, 2018, **66**, 81–92.

125 L. Xia, Z. Yin, L. Mao, X. Wang, J. Liu, X. Jiang, Z. Zhang, K. Lin, J. Chang and B. Fang, *Sci. Rep.*, 2016, **6**, 22005.

126 S. Weiner, W. Traub and H. D. Wagner, *J. Struct. Biol.*, 1999, **126**, 241–255.

127 S. A. Mirmohammadi, D. Pasini and F. Barthelat, *J. Mech. Behav. Biomed. Mater.*, 2022, **134**, 105369.

128 S. Deville, E. Saiz and A. P. Tomsia, *Biomaterials*, 2006, **27**, 5480–5489.

129 D. Li, W. Y. Lai, Y. Z. Zhang and W. Huang, *Adv. Mater.*, 2018, **30**, 1704738.

130 C. S. Luo, P. Wan, H. Yang, S. A. A. Shah and X. Chen, *Adv. Funct. Mater.*, 2017, **27**, 1606339.

131 W. S. Cheong, Y. H. Kim, J. M. Lee, C. H. Hong, H. Y. Choi, Y. J. Kwak, Y. J. Kim and Y. S. Kim, *Adv. Mater. Technol.*, 2019, **4**, 1800550.

132 L. Zhang, D. Wang, F. Liu, H. Wu, G. Pan, H. Wu, Z. Hao and J. Zhang, *Adv. Opt. Mater.*, 2023, 2301114.

133 A. Puszka and J. W. Sikora, *Polymers*, 2022, **14**, 2933.

134 L. Wondraczek, J. C. Mauro, J. Eckert, U. Kühn, J. Horbach, J. Deubener and T. Rouxel, *Adv. Mater.*, 2011, 4578–4586.

135 T. A. Cheema, A. Lichtner, C. Weichert, M. Böl and G. Garnweitner, *J. Mater. Sci.*, 2012, **47**, 2665–2674.

136 F. Petit, A. Sartieaux, M. Gonon and F. Cambier, *Acta Mater.*, 2007, **55**, 2765–2774.

137 X. Huang, G. Liu, Q. Liu and S. J. Bennison, *Struct. Eng. Mech.*, 2014, **52**, 603–612.

138 J. E. Minor and P. L. Reznik, *J. Struct. Eng.*, 1990, **116**, 1030–1039.

139 J. S. Chan and H. Le Ferrand, *Sustainable Mater. Technol.*, 2022, **31**, e00363.

140 C. Wu, F. Lin, X. Pan, Y. Zeng, G. Chen, L. Xu, Y. Fu, Y. He, Q. Chen and D. Sun, *Adv. Funct. Mater.*, 2023, 2215135.

141 A. Shi, Y. Li, W. Liu, J.-Z. Xu, D.-X. Yan, J. Lei and Z.-M. Li, *Compos. Sci. Technol.*, 2019, **184**, 107858.

142 T. Zhang, J. Sun, L. Ren, Y. Yao, M. Wang, X. Zeng, R. Sun, J.-B. Xu and C.-P. Wong, *Composites, Part A*, 2019, **121**, 92–99.

143 H. Wang, Z. Huang, J. Li, F. Wang, Z. Feng, H. Tian, H. Zhao and L. Li, *Appl. Phys. Lett.*, 2021, **118**, 131903.

144 L. Wang, L. Zhang, A. Fischer, Y. Zhong, D. Drummer and W. Wu, *J. Polym. Eng.*, 2018, **38**, 767–774.

145 F. Yuan, W. Jiao, F. Yang, W. Liu, Z. Xu and R. Wang, *RSC Adv.*, 2017, **7**, 43380–43389.

146 Z. Chen, C. Xu, C. Ma, W. Ren and H. M. Cheng, *Adv. Mater.*, 2013, **25**, 1296–1300.

147 R. Wilson, G. George and K. Joseph, *Materials for Potential EMI Shielding Applications*, Elsevier, 2020, pp. 1–8.

148 A. Iqbal, F. Shahzad, K. Hantanasirisakul, M.-K. Kim, J. Kwon, J. Hong, H. Kim, D. Kim, Y. Gogotsi and C. M. Koo, *Science*, 2020, **369**, 446–450.

149 F. Shahzad, M. Alhabeb, C. B. Hatter, B. Anasori, S. Man Hong, C. M. Koo and Y. Gogotsi, *Science*, 2016, **353**, 1137–1140.

150 A. Iqbal, P. Sambyal and C. M. Koo, *Adv. Funct. Mater.*, 2020, **30**, 2000883.

151 M. Han, C. E. Shuck, R. Rakhmanov, D. Parchment, B. Anasori, C. M. Koo, G. Friedman and Y. Gogotsi, *ACS Nano*, 2020, **14**, 5008–5016.

152 H. Zhang, L. Wang, Q. Chen, P. Li, A. Zhou, X. Cao and Q. Hu, *Mater. Des.*, 2016, **92**, 682–689.

153 M. Naguib, V. N. Mochalin, M. W. Barsoum and Y. Gogotsi, *Adv. Mater.*, 2014, **26**, 992–1005.

154 D. Klemm, F. Kramer, S. Moritz, T. Lindström, M. Ankerfors, D. Gray and A. Dorris, *Angew. Chem., Int. Ed.*, 2011, **50**, 5438–5466.

155 A. Isogai, T. Saito and H. Fukuzumi, *Nanoscale*, 2011, **3**, 71–85.

156 B. Yu, B. Tawiah, L.-Q. Wang, A. C. Y. Yuen, Z.-C. Zhang, L.-L. Shen, B. Lin, B. Fei, W. Yang and A. Li, *J. Hazard. Mater.*, 2019, **374**, 110–119.

157 B. Wang, Y. Zhang, Y. Tao, X. Zhou, L. Song, G. Jie and Y. Hu, *J. Hazard. Mater.*, 2018, **352**, 92–100.

158 M. V. T. da Costa, L. Li and L. A. Berglund, *Mater. Des.*, 2023, **230**, 111947.

159 B. Liang, H. Zhao, Q. Zhang, Y. Fan, Y. Yue, P. Yin and L. Guo, *ACS Appl. Mater. Interfaces*, 2016, **8**, 28816–28823.

160 A. Jackson, J. Vincent and R. Turner, *Compos. Sci. Technol.*, 1989, **36**, 255–266.

161 V. Hahn, P. Rietz, F. Hermann, P. Müller, C. Barner-Kowollik, T. Schlöder, W. Wenzel, E. Blasco and M. Wegener, *Nat. Photonics*, 2022, **16**, 784–791.

162 M. Mirkhalaf, X. Wang, A. Entezari, C. R. Dunstan, X. Jiang and H. Zreiqat, *Appl. Mater. Today*, 2021, **25**, 101168.

163 N. M. Larson, J. Mueller, A. Chortos, Z. S. Davidson, D. R. Clarke and J. A. Lewis, *Nature*, 2023, 682–688.

164 Z. Wang, M. Li, C. Yan, J. Cao, M. Du and H. Deng, *Chem. Eng. J.*, 2023, 145779.

165 F. Wang, C. Liu, H. Yang, H. Wang, H. Zhang, X. Zeng, C. Wang, W. Zhang, W. Lv and P. Zhu, *Addit. Manuf.*, 2023, **63**, 103411.

166 Z. Ding, H. Zreiqat and M. Mirkhalaf, *Mater. Horiz.*, 2022, **9**, 2762–2772.

167 B. F. Winhard, P. Haida, A. Plunkett, J. Katz, B. Domènech, V. Abetz, K. P. Furlan and G. A. Schneider, *Addit. Manuf.*, 2023, **77**, 103776.

168 J. Friemann, B. Dashtbozorg, M. Fagerström and S. Mirkhalaf, *Int. J. Numer. Meth. Eng.*, 2023, **124**, 2292–2314.

169 S. Morsali, D. Qian and M. Minary-Jolandan, *Commun. Mater.*, 2020, **1**, 12.

170 N. Abid, M. Mirkhalaf and F. Barthelat, *J. Mech. Phys. Solids*, 2018, **112**, 385–402.

171 G. Hunter, L. Djumas, L. Brassart and A. Molotnikov, *Mater. Des.*, 2022, **218**, 110680.

172 L. A. Shaw, S. Chizari, M. Dotson, Y. Song and J. B. Hopkins, *Nat. Commun.*, 2018, **9**, 1–12.

173 M. Mirkhalaf and A. Rafsanjani, *Matter*, 2023, DOI: **10.1016/j.mat.2023.08.020**.

174 S. Gantenbein, E. Colucci, J. Käch, E. Trachsel, F. B. Coulter, P. A. Rühs, K. Masania and A. R. Studart, *Nat. Mater.*, 2023, **22**, 128–134.